Author Manuscript

Author Manuscript

Author Manuscript

Author Manuscript

HHS Public Access

Author manuscript

Mol Neurobiol. Author manuscript; available in PMC 2018 September 01.

Published in final edited form as:

Mol Neurobiol. 2017 September ; 54(7): 4936–4952. doi:10.1007/s12035-016-0034-9.

Intranasal Delivery of a Caspase-1 Inhibitor in the Treatment of Global Cerebral Ischemia

Ningjun Zhao[1,2,a], **Xiaoying Zhuo**[1,2,a], **Yujiao Lu**[2], **Yan Dong**[2], **Mohammad Ejaz Ahmed**[2], **Donovan Tucker**[2], **Erin L. Scott**[2], and **Quanguang Zhang**[2,*]

[1]Department of Emergency Medicine, Xuzhou Medical University, and Laboratory of Emergency Medicine, the affiliated Hospital of Xuzhou Medical University, Xuzhou, Jiangsu 221002, China

[2]Department of Neuroscience and Regenerative Medicine, Augusta University, Augusta, Georgia 30912, USA

Abstract

Caspase-1 is an enzyme implicated in neuroinflammation, a critical component of many diseases that affect neuronal degeneration. However, it is unknown whether a caspase-1 inhibitor can modify apoptotic neuronal damage incurred during transient global cerebral ischemia (GCI) and whether intranasal administration of a caspase-1 inhibitor is an effective treatment following GCI. The present study was conducted to examine the potential efficiency of post-ischemic intranasal administration of the caspase-1 inhibitor Boc-D-CMK in a 4-vessel occlusion model of GCI in the rat. Herein, we show that intranasal Boc-D-CMK readily penetrated the central nervous system, subsequently inhibiting caspase-1 activity, decreasing mitochondrial dysfunction, and attenuating caspase-3 dependent apoptotic pathway in ischemia-vulnerable hippocampal CA1 region. Further investigation regarding the mechanisms underlying Boc-D-CMK's neuroprotective effects, revealed marked inhibition of reactive gliosis, as well as reduction of the neuroinflammatory response via inhibition of the downstream pro-inflammatory cytokines production. Intranasal Boc-D-CMK post-treatment also significantly enhanced the numbers of NeuN-positive cells while simultaneously decreasing the numbers of TUNEL-positive and PARP1-positive cells in hippocampal CA1. Correspondingly, behavioral tests showed that deteriorations in spatial learning and memory performance, and long-term recognition memory following GCI were significantly improved in the Boc-D-CMK post-treated animals. In summary, the current study demonstrates that the caspase-1 inhibitor Boc-D-CMK coordinates anti-inflammatory and anti-apoptotic actions to attenuate neuronal death in the hippocampal CA1 region following GCI. Furthermore, our data suggest that pharmacological inhibition of caspase-1 is a promising neuroprotective strategy to target ischemic neuronal injury and functional deficits following transient GCI.

[*]Corresponding Author: Quanguang Zhang, Ph.D., Associate Professor, Department of Neuroscience and Regenerative Medicine, Medical College of Georgia, Augusta University, 1120 15th Street, CA3050, Augusta, GA 30912, USA, Phone: (706) 721-7025; Fax: (706) 721-8685;, qzhang@augusta.edu.

[a]Ningjun Zhao and Xiaoying Zhuo contributed equally to this work.

Statement of interest

The authors declare that there is no conflict of interest in the current study.

Author Manuscript Author Manuscript Author Manuscript Author Manuscript

Keywords

Cardiac arrest; Mitochondria; Gliosis; Neuroprotection; Functional improvements

Introduction

Approximately 326,000 ambulatory and 209,000 hospitalized patients experience cardiac arrest annually in the United States [1]. Unfortunately, despite regular updates of cardiopulmonary resuscitation guidelines, treatment outcomes of cardiac arrest remain poor, with less than 9% of cardiac arrest patients reported as surviving with good neurological function [1]. Cardiac arrest and resuscitation induces transient global cerebral ischemia (GCI) followed by ischemic reperfusion (I/R) injury [2,3], and brain injury is the predominant cause of high morbidity and mortality. The brain is particularly susceptible to GCI from cardiac arrest, as the abrupt cessation of blood flow drastically reduces the oxygen and glucose supply to the brain tissue, causing severe ischemic neuronal injury, especially in the vulnerable hippocampal CA1 region [4,5]. This type of neuronal death in hippocampal CA1 starts 2–3 days after reperfusion and mature at 7 days after the insult, which is well known as apoptotic neuronal cell death [6–8]. Along these lines, survival of cardiac arrest is often complicated by persistent cognitive impairment, such as memory and sensorimotor deficits, which subsequently leads to poor quality of life and heavy economic burden [9]. In spite of our increased awareness of ischemic brain injury following GCI, the underlying mechanisms remain unclear, and the clinical therapeutic strategies for effective treatments remain ineffective. Therefore, it is important to further study transient GCI in order to better understand the mechanisms of hippocampal CA1 neuronal damage, as it will yield vital information that may direct the development of better treatment strategies.

Neuro-inflammation plays a pivotal role in many diseases that affect the central nervous system, including transient GCI, and the pro-inflammatory cytokines interleukin 1β (IL-1β) and interleukin 18 (IL-18), are thought to have particular importance [10–12]. Caspase-1, also known as IL-1β-converting enzyme, converts IL-1β and IL-18 from their inactive precursors into active molecules via proteolytic cleavage. Consequently, caspase-1 has become synonymous with inflammation because it is thought to act as a key mediator of inflammatory processes [13–15]. However, in addition to facilitating neuroinflammation, caspase-1 plays an additional role as an apoptotic protease. In fact, a large body of literature reports that caspase-1 is directly involved in non-infectious cell death processes [16–20]. Along these lines, genetic knockout or pharmacological inhibition of caspase-1 in mice reduces ischemia-induced brain injury in models of stroke, and improves post-ischemic neurologic outcomes [21–23]. Research has also shown that caspase-1 inhibitors are neuroprotective against neuronal death in rat organotypic hippocampal CA1 slices and that this effect is not a result of the inhibition of IL-1β production [24]. Unfortunately, no studies have yet verified the potent beneficial effects of a caspase-1 inhibitor on ischemic cerebral injury sustained from transient GCI *in vivo*. Thus, for the present study, we hypothesized that inhibition of caspase-1 with the caspase-1 inhibitor Boc-D-CMK may afford neuroprotection against brain injury in a rat model of GCI.

Author Manuscript Author Manuscript Author Manuscript Author Manuscript

It is currently unknown whether a caspase-1 inhibitor can modulate the inflammatory response, apoptotic neuronal damage, and functional improvements that following GCI. To address this knowledge gap, the goals of the present study were: (1) to assess whether the caspase-1 inhibitor Boc-D-CMK attenuates neuroinflammation in the hippocampus following transient GCI, (2) to evaluate whether the caspase-1 inhibitor Boc-D-CMK affects caspase-3 dependent apoptotic pathway in the hippocampal CA1 in a rat model of transient GCI, and (3) to determine whether the caspase-1 inhibitor Boc-D-CMK ameliorates functional neurological impairment induced by GCI in rats. An additional aim of the current study was proof of concept that *intranasal* administration of the caspase-1 inhibitor Boc-D-CMK is safe and effective in adult rats subjected to a 4-vessel occlusion model of GCI.

Materials and Methods

Animals and Global Cerebral Ischemia (GCI)

Male Sprague Dawley rats (250–280 g, Charles River Laboratories) were randomly divided into three groups: (a) Sham control group, (b) GCI group with vehicle infusion, (3) GCI group with Boc-D-CMK treatment. All animals except the sham group were subjected to the 4-vessel occlusion model of GCI, as previously described by our laboratory [25]. Briefly, animals were anesthetized using pentobarbital sodium (Diamondback Drugs, 40 mg/kg, Intraperitoneal injection), and the vertebral arteries were permanently occluded at the level of the alar foramina using electrocautery. Next, both common carotid arteries (CCAs) were isolated, and a silastic ligature was placed loosely around each artery without interrupting the blood flow. The incisions were then closed by wound clips. After a 24-h recovery period, bilateral CCAs were exposed under light anesthesia, and GCI was induced by occluding the CCAs for 15 min with aneurysm clips. At the end of the ischemic period, the clips were removed, and blood flow through the arteries was confirmed before the wound was closed. Rectal temperature was maintained at 36.5 to 37.5°C throughout the experiment via a thermal blanket and an infrared lamp. The animals in the sham group underwent identical procedures except that the CCAs were simply exposed but not occluded. All procedures were approved by the University Institutional Animal Care and Use Committee and were in compliance with National Institutes of Health guidelines.

Intranasal Drug Administration

Boc-D-CMK (AnaSpec, Inc., Fremont, CA) was administered via intranasal drops. Rats were anesthetized and placed in a supine position, which held their noses at an upright, 90°-angle [26,27]. Then, Boc-D-CMK (5 μg/μl), was administered in nose drops (2.5 μL/drop) by a pipette over a period of 20 min, alternating drops every 4 to 5 minutes between the left and right nares, for a total volume delivered of 20 μl. An identical volume of vehicle (5% DMSO in saline) was given by intranasal administration in the I/R control group. Intranasal administration of Boc-D-CMK or vehicle was performed at 2 and 24 h after initiating reperfusion following GCI. The optimal and effective doses of this caspase-1 inhibitor were confirmed in a preliminary study in our laboratory. All animals were maintained in a supine position for 60 min after intranasal administration. Biotin-labeled caspase-1 inhibitor or vehicle buffer was delivered intranasally to a subset of rats in order to determine hippocampal drug localization, and the rats were sacrificed 12 h after drug administration. A

Author Manuscript Author Manuscript Author Manuscript Author Manuscript

Streptavidin Alexa Fluor 488 conjugated antibody (Thermo Fisher Scientific Inc.) was then used for confocal microscopy to visualize the caspase-1 inhibitor within the brain.

Histology Analyses

Histological examination was performed as previously described [28]. All animals were deeply anesthetized and subjected to transcardial perfusion with 0.9% saline, followed by cold 4% paraformaldehyde in 0.1 M phosphate-buffered saline (PBS). Brains were removed and post-fixed, and cryoprotected with 30% sucrose at 4 °C until they sank. Coronal sections (25 μm) were cut on a Leica RM2155 microtome and collected throughout the entire dorsal hippocampus. For histological assessment, brain sections were stained with 0.01% (w/v) Cresyl Violet for 10 min, followed by graded ethanol dehydration. The stained sections were examined, and images were captured using an AxioVision4Ac microscope system (Carl Zeiss, Germany). For confocal staining, the sections were washed for 20 min in 0.1% PBS-Triton-X100. After incubation with a blocking solution containing 10% donkey serum for 1 h at room temperature, sections were incubated with mouse anti-NeuN monoclonal antibody (1:500, EMD Millipore, Billerica, MA) overnight at 4°C. The sections were then washed 3 times, followed by incubation with Alexa Fluor 568 donkey anti-mouse antibody (1:500, Thermo Fisher Scientific) for 1 h. Thereafter, sections were washed and the sections were mounted using Vectashield mounting medium with 4', 6-diamidino-2-phenylindole (DAPI) (H-1200; Vector Laboratories, Inc., CA, USA), and a coverslip was added. Three to five sections from each animal (200 μm apart, approximately 1.5–3.3 mm posterior to Bregma) were selected for confocal microscopy and imaged using a Zeiss LSM510 Meta confocal laser microscope (Carl Zeiss) using 40× objective lens with the image size set at 1024 × 1024 pixels. The captured images were then processed and analyzed by the LSM 510 META software. TUNEL staining was performed on free-floating coronal sections using the Click-iT® Plus TUNEL assay kit (Thermo Fisher Scientific), according to the manufacturer's instructions. For a negative control, some slides were incubated with the label solution without terminal transferase for TUNEL. The number of TUNEL--positive cells and NeuN-positive cells per 250 μm length of medial CA1 pyramidal cell layer was counted bilaterally. Cell counts from the right and left hippocampus on each of the sections were averaged to provide the mean value as described previously [25,28].

Immunofluorescence Staining

The coronal sections (25 μm) were incubated with 10% normal donkey serum for 1 h at room temperature in PBS containing 0.1% Triton X-100, followed by incubation with appropriate primary antibodies overnight at 4°C in the same buffer. The following primary antibodies were used in different combinations: anti-NeuN (1:500, Millipore, MA), Iba1, GFAP and PARP1 (1:200, Proteintech, IL), Caspase-1 and Cle-caspase-1 (1:50, Santa Cruz Biotechnology), Cle-caspase-3 and Cle-caspase-9 (1:50, Cell Signaling Technology). After primary antibody incubation, the sections were washed 4 times for 10 min at room temperature, followed by incubation with the appropriate combination of Alexa Fluor donkey anti-mouse/rabbit/goat secondary antibody (1:500, Thermo Fisher Scientific) for 1 h at room temperature. For negative control staining, the primary antibody was omitted during immunostaining. The sections were then washed, mounted and coverslipped in Vectashield mounting medium (H-1200, Vector Laboratories). Three to five sections from each animal

Author Manuscript Author Manuscript Author Manuscript Author Manuscript

(200 μm apart) were selected for confocal microscopy. The captured images were processed and analyzed using LSM510 Meta imaging software.

Tissue preparation and Western Blotting Analysis

For brain tissue preparation, rats were sacrificed under deep anesthesia at the time points stated in the experiments, and whole brains were quickly removed. The hippocampal CA1 regions were then rapidly microdissected from both sides of the hippocampal fissure and immediately frozen. The samples were homogenized as previously described by our laboratory [29]. Briefly, tissues were homogenized in ice cold homogenization medium consisting of 50 mM HEPES (pH 7.4), 150 mM NaCl, 12 mM β-glycerophosphate, 3 mM dithiotheitol (DTT), 2 mM sodium orthovanadate (Na3VO4), 1 mM EGTA, 1 mM NaF, 1 mM phenylmethylsulfonyl fluoride (PMSF), 1% Triton X-100 and inhibitors of proteases and enzymes (Thermo Scientific, Rockford, IL) with a Teflon-glass homogenizer. The homogenates were centrifuged at 12,000 ×g for 30 min at 4°C, and the supernatants (total protein fractions) were collected and stored at −80°C until use. As necessary, the subcellular cytosolic fractions and mitochondrial fractions were prepared as described in our previous work PMID: 25462588. Briefly, tissues were homogenized in a buffer containing 10 mM HEPES (pH 7.9), 0.6% NP-40, 12 mM β-glycerophosphate with inhibitors of proteases and enzymes. The homogenates were centrifuged at 800 × g for 10 min, and the resulting supernatants were further centrifuged at 17,000 × g for 20 min at 4°C to yield cytosolic fractions in the supernatants and mitochondrial fractions in the pellets. Protein concentrations were determined via Modified Lowry Protein Assay (Pierce, Rockford, IL), and the samples were aliquoted and stored at −80 °C until use. For Western blotting analysis, 50 μg of proteins were separated on 4–20% sodium dodecyl sulfate-polyacrylamide gel electrophoresis and transferred to PVDF membrane. The membranes were blocked and incubated with primary antibody at 4 °C overnight and probed by incubation with HRP-conjugated secondary antibodies for 1 h at room temperature. The following primary antibodies were used in this study: COX4, Caspase-1 and Cle-caspase-1 (1:200, Santa Cruz Biotechnology), Iba1, Cytochrome c, GFAP and GADPH (1:1000, Proteintech, IL). Bound proteins were visualized using a CCD digital imaging system (HM3050A, Zhanglab). Band densities were normalized to the loading control of GAPDH or COX4 signals, and analyzed with the ImageJ analysis software (Version 1.49; NIH, USA). A Mean±SE was calculated from the data for all animal groups for graphical presentation and statistical comparison.

Caspase Activity Measurement

Activity levels for caspase-9 and caspase-3 were measured in the total protein samples from CA1 region using luorometric substrates, as previously described as described by our laboratory [30]. The substrates for caspase-3 and caspase-9 were Ac-DEVD-AMC and Ac-LEHD-AMC (AnaSpec, Fremont, CA), respectively. The fluorescence of free AMC was determined with an excitation wavelength of 360 nm and an emission wavelength of 460 nm with a Microplate reader (BioTek Instruments). Chromogenic caspase-1 substrate (Ac-YVAD-pNA, AnaSpec) was used to measure caspase-1 activity using the total protein samples from CA1 region, according to the vendor's instructions. Caspase-1 activity was determined colorimetrically by measuring the cleavage of pNA peptide at 408 nm absorbance using a spectrophotometer (Bio-Rad Benchmark Plus, Microplate

Author Manuscript Author Manuscript Author Manuscript Author Manuscript

Spectrophotometer). Values were expressed as percentage changes versus sham group for graphical depiction.

Mitochondrial Cytochrome C Oxidase Activity

Cytochrome c oxidase activity was assessed using mitochondrial fractions with an activity assay kit (ab109911; Abcam Inc) according to the manufacturer's instructions. The ability of cytochrome c oxidase to oxidize fully reduced ferro-cytochrome c to ferri-cytochrome c was measured colorimetrically. The absorbance of oxidized cytochrome c was measured at 550 nm absorbance in a 96-well plate using a spectrophotometer (Bio-Rad Benchmark Plus). The data presented were calculated as percentage changes versus control group.

Mitotracker Red Staining and Confocal Microscopy

MitoTracker® Red CMXRos (M-7512, Life Technologies, NY, USA), a red fluorescent dye, was used to measure depolarization of MMP, as described recently [30]. In brief, 5 min after intraperitoneal injection of MitoTracker® Red (50 ng/ml in 100 μl of saline), the animals 2 days after GCI were deeply anesthetized with isoflurane and transcardially perfused with 0.1 M PBS, followed by 4% paraformaldehyde. Brains were removed, post-fixed and cryoprotected with 30% sucrose at 4 °C. Frozen coronal sections (25 μm) were prepared, mounted and coverslipped in Vectashield mounting medium with DAPI (H-1200; Vector Laboratories). Three to five sections of each animal (200 μm apart) were selected and images were acquired on an LSM510 META confocal laser microscope (Carl Zeiss). The fluorescence signals of MitoTracker Red were quantitatively evaluated using ImageJ software, and the intensities were normalized as percentage changes compared with sham control group. Data are presented as Mean ± SE from four to five independent animals per group.

Pro-inflammatory Cytokine Assays

Indirect Enzyme-Linked Immunosorbent Assay (ELISA) assay was used to test the levels of pro-inflammatory cytokines in the total protein samples from hippocampal CA1 3 days after GCI [31]. In brief, 30 μg protein samples from each animal were diluted to 50 μL with bicarbonate/carbonate coating buffer (Sigma-Aldrich). The samples were loaded in PVC ELISA microplates (Corning) and incubated overnight at 4°C. After washing, the plate wells were blocked for 2 h at room temperature using 1% BSA blocking buffer. Then, specific antibodies against IL-1β, IL-18, TNF-α and IL-6 were added and incubated for 2 h at 37°C. Plate wells were then washed and incubated with HRP-conjugated secondary antibodies for 1 hour at room temperature. Finally, the wells were washed three times and developed by incubation with TMB (3,3',5,5'-tetramethylbenzidine, Thermo fisher) for 30 min at room temperature. The reaction was stopped by the addition of sulfuric acid, and optical density was read at 450 nm on a spectrophotometer (Bio-Rad). Data were calculated and expressed as percent change compared with sham control group.

Barnes Maze

The Barnes maze test, which has been widely used to assess hippocampal-dependent spatial learning and memory [32,33], was performed as previously described by our laboratory [30].

Author Manuscript Author Manuscript Author Manuscript Author Manuscript

The Plexiglas apparatus used is a 122 cm-diameter circular platform on a 1.0 m stand with 18 evenly spaced 10 cm-diameter holes around the circumference with a black escape box (20×15×12 cm) placed underneath one of the holes. Several static visual cues were placed on the black walls surrounding the platform to optimize cognitive performance. Testing was performed in a darkened room with bright flood incandescent light (500W, 1000 lux) shining down on the maze surface. Rats were also exposed to noxious auditory stimulus with the use of digital metronome software and two computer speakers facing the platform. Training trials were performed on day 8, 9 and 10 after GCI, during which the rat was placed in the center of the maze, and the rat was allowed 180 s to locate the escape box. If the rat did not find and enter the escape box within the time limit, it was guided to the box and allowed 30 s inside before being returned to its home cage. Each rat was tested once per day. The time to enter into the target hole was recorded using an overhead camera controlled by ANY-maze video tracking software (Stoelting Co., Wood Dale, IL). The probe trial was performed on day 11 after GCI. The escape box was removed and the time spent in the target quadrant was recorded during a 90-second period. The platform and escape box were cleaned with 70% ethanol and dried with a blower fan between each test. The escape latency and the time spent in target quadrant were analyzed using ANY-maze software.

Novel Object Recognition Task

Based on the spontaneous tendency of rodents to spend more time exploring a novel object than a familiar one [34], the Novel Object Recognition (NOR) task is commonly used to evaluate recognition memory in animal models of central nervous system (CNS) disorders [35,36]. The NOR apparatus and procedures have been described before in a rat model [37]. NOR task test was conducted in a open-field arena (40×50×50cm) with two identical objects fixed to the floor (Fig. 10). One day before test, all animals were given a habituation session, in which they were left to freely explore the empty box for 5 min. On day 12 after GCI (sampling day), the animal were exposed to the familiar arena with two identical objects placed at an equal distance. After 5 min, the rat was removed from the object recognition box and returned to its home cage. The next day (choice day), the animal was allowed to explore the open field in the presence of one familiar object and a novel object. The time spent exploring each object was recorded using ANY-maze video tracking software as mentioned above. Exploration of the object was defined as the animal's nose being in the zone at a distance of < 2 cm. The Recognition Index (RI), or the percent of time spent exploring the novel object relative to the total time spent exploring both objects, was calculated and used as the main index of retention in NOR [38,39].

Statistical Analysis

All data are presented as mean±SE. Statistical analysis was performed using one–way, two-way analysis of variance (ANOVA), or Student's t-test with SigmaStat 3.0 software (SPSS, Inc., Chicago, IL), as dictated by experimental design. All the analyses were followed by Student-Newman-Keuls post hoc tests (for all pairwise comparisons) or Dunnett's post-hoc tests (for multiple comparisons versus a control), as appropriate. Statistical significance was accepted at the 95% confidence level.

Author Manuscript Author Manuscript Author Manuscript Author Manuscript

Results

Characterization of caspase-1 protein expression in hippocampal CA1 region of adult male SD rats following GCI

While both pharmacological inhibition and genetic knockout of caspase-1 has been shown to be neuroprotective in the middle cerebral artery occlusion (MCAO) model of cerebral ischemia in mice [21,22], little is known about hippocampal caspase-1 expression following GCI in rats. First, we determined the basal expression of caspase-1 protein in the hippocampal CA1 region of sham-operated rats, which did not undergo ischemia. As shown in Fig. 1A and B, Immunofluorescence staining for caspase-1 (Casp-1, green), MAP2 (red) and GFAP (red) revealed high levels of immunoreactive caspase-1 staining in the hippocampal CA1 pyramidal meurons. Intriguingly, caspase-1 immunostaining was found to colocalize both with the neuronal marker MAP2 and the astrocyte marker GFAP, suggesting that caspase-1 is expressed in both neurons and astrocytes in the rat brain at baseline. We next performed immunofluorescence staining for the same markers in adult rats subjected to GCI. Compared to the basal distribution of caspase-1 immunostaining in the hippocampal CA1 region seen in sham-operated animals, confocal analysis demonstrated statistically significant overexpression of caspase-1 protein in astrocytes both 3 days (a time point neurons start to die) and 14 days (a time point neuronal death is mature) following GCI (Fig. 1C).

Neural distribution of biotin-labeled caspase-1 inhibitor after intranasal administration

To demonstrate that an intranasally administered caspase-1 inhibitor could bypass the blood-brain-barrier and reach the hippocampus, a subset of rats were sacrificed at 12 h after intranasal delivery of a biotin-labeled caspase-1 inhibitor. As seen in Fig. 2A (a–c), the Biotin-labeled caspase-1 inhibitor successfully penetrated the rat brain after intranasal administration, with a significant portion reaching the ischemia-vulnerable hippocampal CA1 region. Furthermore, confocal microscopy showed that the intranasally delivered caspase-1 inhibitor mainly localized to the cellular cytoplasm of neurons in the hippocampal CA1 and the cortex. In contrast, control group received vehicle buffer intranasally showed negligible fluorescent signal (green). This serves as poof of concept that a caspase-1 inhibitor can penetrate the central nervous system via the nasal cavity, effectively circumventing the blood-brain barrier through intranasal delivery.

Intranasal Boc-D-CMK post-treatment inhibits GCI-induced caspase-1 overexpression, cleavage, and activity in hippocampal CA1 region

To determine whether intranasal Boc-D-CMK post-treatment can exert neuroprotective effects on a GCI rat model, we initially measured the time course of caspase-1 activity in the hippocampal CA1 region after transient GCI using a caspase-1 chromogenic substrate assay. Compared to sham-operated animals, caspase-1 activity was increased at all time points observed after ischemia, reaching a peak level at 3 days post GCI and remaining at a high level by 5 days post GCI (Fig. 2B). Confocal microscopy revealed that the cleaved-caspase-1 (active form) was markedly increased and co-localized to astrocytes 3 days post GCI (Fig. 2C) compared with sham controls. By contract, the expression and localization of cleaved-caspase-1 were drastically decreased in Boc-D-CMK treated animals. Importantly, intranasal

Author Manuscript Author Manuscript Author Manuscript Author Manuscript

Boc-D-CMK post-treatment significantly decreased the activity of caspase-1 in hippocampal CA1 region 3 days following GCI, in comparison with the I/R control group (Fig. 2D). Western blotting demonstrated that the expression of caspase-1 and cleaved-caspase-1 were both significantly increased in the hippocampal CA1 region 3 days after GCI, and the increased expression levels were effectively suppressed by intranasal Boc-D-CMK treatment (Fig. 2E).

Intranasal Boc-D-CMK post-treatment improves GCI-induced mitochondrial dysfunction in hippocampal CA1 region

Mitochondria serve as a latent major intracellular source of reactive oxygen species (ROS) in neurons, and their dysfunction subsequently contributes to the increase in oxidative stress observed following ischemia [40,41]. We have confirmed in our previous work that day 2 after GCI is a good reperfusion time point to detect mitochondrial membrane potential (MMP) [30]. In the present study, we examined whether the caspase-1 inhibitor Boc-D-CMK has the ability to prevent mitochondrial dysfunction in the vulnerable hippocampal CA1 region following I/R. As shown in Fig. 3A, MMP in CA1 hippocampal neurons was examined under confocal microscopy using the fluorescence changes of MitoTracker Red fluorescent dye. In healthy pyramidal neurons of the CA1 cell layer of sham animals, mitochondria labeled with Mitotracker Red exhibited strong fluorescence. The intensities of MitoTracker Red fluorescence signals were quantitatively evaluated and normalized as percentage changes compared to the sham group. As shown in Fig. 3B, the normalized Mitotracker Red fluorescence, in the cytoplasm of hippocampal CA1 pyramidal neurons, was significantly decreased 2 days after GCI, suggesting a GCI-induced mitochondrial depolarization and potential collapse of the MMP. Intriguingly, intranasal Boc-D-CMK post-treatment reversed the GCI-induced change in Mitotracker Red fluorescence intensity, compared with I/R group, indicating a preservation of MMP and the presence of healthy mitochondria. Further analysis of mitochondrial cytochrome c oxidase activity demonstrated that GCI resulted in a significant inhibition of mitochondrial cytochrome c oxidase activity in hippocampal CA1 region 2 days post I/R, indicating dysfunction of mitochondrial electron transfer chain following GCI. Interestingly, intranasal Boc-D-CMK post-treatment significantly increased cytochrome c oxidase activity, relative to I/R group (Fig. 3C). Western blotting and data analyses further indicated that Boc-D-CMK attenuated GCI-induced release of mitochondrial cytochrome c, as evidenced by decreased cytosolic level of cytochrome c and increased mitochondrial level of cytochrome c 2 days after GCI (Fig. 3D). Taken together, these data suggest that intranasal Boc-D-CMK post-treatment has the ability to preserve MMP and rescue GCI-induced mitochondrial dysfunction in CA1 region following I/R.

Intranasal Boc-D-CMK post-treatment suppresses caspase-9 and caspase-3 activation in hippocampal CA1 region

The cleavage and subsequent activation of caspase-9 and caspase-3 plays a pivotal role in the execution phase of cell apoptosis [13]. Along these lines, one major consequence of mitochondrial dysfunction and subsequent release of cytochrome c is the activation of caspase-9 and the activation of caspase-3. Thus, we aimed to determine whether the potential neuroprotective property of Boc-D-CMK further involved the inhibition of

Author Manuscript Author Manuscript Author Manuscript Author Manuscript

caspase-9 activation, inhibition of caspase-3 activation, and subsequent inhibition of apoptotic cell death. As shown in Fig. 4A and 4B, 3-day I/R evoked significant increases in the activities of caspase-9 and caspse-3. Importantly, the increased activities were dramatically prevented in Boc-D-CMK-treated animals. In addition, the expressions and localizations of cleaved-caspase-3 and cleaved-caspase-9 were examined by double immunofluorescence staining with NeuN on the brain sections 3 days after I/R. Representative confocal microscopy imaging and analysis certified that, there were significant increases in cleaved-caspase-3 and cleaved-caspase-9 immunostainings compared to sham, which co-localized with NeuN-positive cells, in the I/R group (Fig. 4C and 4D). Meaningfully, Boc-D-CMK post-treatment markedly attenuated the neuronal localizations of cleaved-caspase-9 and cleaved-caspase-3 compared to I/R control group.

Intranasal Boc-D-CMK post-treatment inhibits the intrinsic apoptotic pathway in hippocampal CA1 region following GCI

We next analyzed the effects of caspase-1 inhibition on GCI-induced apoptotic cell death of hippocampal CA1 neurons following GCI. Coronal brain sections from sham animal and animals after 3-day ischemic reperfusion were subjected to TUNEL staining and poly-ADP polymerase 1 (PARP1) staining. As shown in Fig. 5A, immunofluorescence staining indicated that, 3-day ischemic reperfusion induced remarkable TUNEL and PARP1 staining in the hippocampal CA1 cell layer, compared with sham and Boc-D-CMK treated groups. Quantitative analysis showed that the number of TUNEL-positive and PARP1-positive cells in the CA1 pyramidal cell layer was significantly attenuated in the Boc-D-CMK post-treated animals compared with the I/R animals, indicating that Boc-D-CMK has the ability to inhibit the intrinsic apoptotic neuronal death following GCI.

Intranasal Boc-D-CMK post-treatment attenuates GCI-induced microglial activation and astrocytosis following GCI in hippocampal CA1 region

To investigate whether caspase-1 pathway was involved in reactive gliosis following ischemic reperfusion, we first examined the glial activation at the early time point (day 3) following ischemic reperfusion. Western blotting and quantification analyses of Iba1 and GFAP in total protein samples from hippocampal CA1 region showed that the Iba1 and GFAP levels were significantly increased compared with sham control groups 3 days after GCI, suggesting GCI-induced reactive gliosis (Fig. 6A). Interestingly, Boc-D-CMK treated animals exhibited robust decreases in the levels of Iba1 and GFAP versus I/R control group. In order to analyze microglial and astrocyte activation occurring at the late time point after GCI, the brain sections 14 days after GCI were selected for Iba1 and GFAP staining. As shown in Fig. 6B and 6C, immunofluorescence staining and relative intensity analyses indicated that the microglial activation and astrocytosis were dramatically enhanced 14 days post GCI in rat hippocampal CA1 region, compared to the sham group. As excepted, GCI-induced reactive gliosis was significantly reduced in the Boc-D-CMK treatment group, compared to the I/R group 14 days post GCI.

Author Manuscript Author Manuscript Author Manuscript Author Manuscript

Intranasal Boc-D-CMK post-treatment inhibits GCI-induced production of pro-inflammatory cytokines in hippocampal CA1 region

As a potent inducer of inflammation, IL-1β is synthesized as an inactive precursor, pro-IL-1β, which requires two activating steps to induce its cleavage and facilitate its maximal activity. Cleavage of pro-IL-1β is typically performed by the cysteine protease caspase-1 to produce a 17-kDa mature IL-1β [42]. In addition to pro–IL-1β maturation, caspase-1 is also involved in the maturation of inflammatory cytokines IL-18, IL-6, and TNF-α [43]. In the present study, IL-1β, IL-18, IL-6 and TNF-α were measured with highly sensitive ELISAs using hippocampal CA1 protein homogenates from each group 3 days after GCI. As indicated in Fig. 7A–7D, the levels of IL-1β, IL-18, IL-6 and TNF-α were all increased significantly in the ischemic control group compared to sham animals. However, intranasal Boc-D-CMK post-treatment markedly reduced the secretion of all inflammatory cytokines tested. These data suggest that the caspase-1 inhibitor Boc-D-CMK attenuated neuroinflammation in the CA1 hippocampal region following GCI by preventing maturation of inflammatory cytokines.

Intranasal Boc-D-CMK post-treatment prevents GCI-induced delayed neuronal cell death in hippocampal CA1 region

We next evaluated whether Boc-D-CMK post-treatment is able to protect against GCI-induced delayed neuronal cell death in the hippocampal CA1 region. Histological evaluation via Cresyl Violet staining and NeuN staining confirmed that transient GCI induced profound local neuronal loss in the ischemia-vulnerable hippocampal CA1 region in the I/R animals, compared to sham groups (Fig. 8A–8C, second Panel). Cresyl Violet-stained sections from animals of the I/R group showed unequivocal signs of cell death 14 days after GCI, as the pyramidal cells had condensed, pyknotic, and shrunken nuclei. In contrast, histology and quantitative analysis showed that intranasal Boc-D-CMK post-treatment significantly increased the number of surviving neurons in the hippocampal CA1 region 14 days following GCI (Fig. 8A–8C, third Panel), compared to the non-treated I/R group. These results demonstrate the strong neuroprotective effects of intranasal Boc-D-CMK post-treatment against the selective delayed neuronal cell death in the hippocampal CA1 region following transient GCI.

Boc-D-CMK post-treatment attenuates GCI-induced spatial learning and memory deficits

The Barnes maze test is widely used to assess hippocampal-dependent spatial learning and memory [44,45]. The hippocampus, CA1 region in particular, plays an important role in the processing of spatial locations [46]. We have found in the recent study that rats with ischemic hippocampal injury have impaired performance of spatial learning and long-term memory in the Barnes maze task [30]. Thus, to determine whether the neuroprotective effects of Boc-D-CMK correlate with functional improvement, the animals in each group were subjected to Barnes maze as described in Methods. Training trials of all animals were performed on days 8, 9 and **10** after GCI, and a probe trial were performed on day **11** after GCI. As shown in Fig. 9A and 9B, the I/R control animals took more time to locate the black escape box during training trials on day 10 after GCI, compared to sham-operated animals. Interestingly, Boc-D-CMK treated animals showed significantly decreased escape

Author Manuscript Author Manuscript Author Manuscript Author Manuscript

latencies to find the escape box on the final day of training trials. In the probe test on day 11 after GCI, the I/R control animals spent significantly less time in the target quadrant (where the escape box had been) than the Boc-D-CMK-treated animals and the sham animals (Fig. 9C and 9D). These data suggest that the caspase-1 ihibitor Boc-D-CMK has the ability to significantly attenuate long-term learning and memory impairment following GCI.

Boc-D-CMK post-treatment enhances recognition memory in Novel Object Recognition test

While the hippocampus is well-known to be important for spatial memory, its integrity is also necessary for non-spatial tasks, such as object recognition memory [47]. Along these lines, we investigated whether intranasal Boc-D-CMK post-treatment would improve recognition deficits induced by I/R after transient GCI. The NOR task was performed as described in Methods to test the long-term recognition memory of the animals in each group. Fig. 10A demonstrates the representative tracks from the sampling session on day 12 after GCI and the choice session at day 13 after GCI. As seen in Fig. 10A and 10B, there was no significant difference in the recognition index among all groups in the sampling session on day 12 after I/R. Intriguingly, the recognition index in the Choice session on day 13 was significantly decreased in the I/R control group, and the decrease was effectively reversed in the Boc-D-CMK-treated animals after I/R (Fig. 10B and 10C). The results demonstrated the effectiveness of caspase-1 inhibition in improving long-term recognition memory following GCI.

Discussion

Thus far, no effective treatment for post-cardiac arrest cerebral I/R injury exists. In addition to the sheer complexity of mechanisms underlying the response to cerebral I/R, another intractable obstacle is the presence of the blood brain barrier (BBB), which limits pharmacological CNS penetration and subsequently restricts the application of many therapeutic agents that could target neuroinflammation and neurodegeneration. Invasive methods of administration used to bypass the BBB, such as itrathecal injections or intracerbroventricular (i.c.v.) injections, are not practical for routine clinical use. In contrast, the nasal mucosa affords an easily accessible, non-invasive method of rapidly delivering CNS-targeted therapeutics, which conveniently allows for circumvention of the first-pass metabolism as well. Growing evidence suggests that intranasal administration of drug therapy is effective in animal models of Alzheimer's disease and stroke [48–50]. Caspase-1 is known to be a vital mediator of inflammatory processes that is also directly involved in non-infectious cell death processes [16,13,14,19]. In the current study, we demonstrate via confocal microscopy that intranasal administration of a Biotin-labeled caspase-1 inhibitor *in vivo* leads to distribution of the drug throughout the cerebral cortex and the hippocampal CA1 region, which is particularly vulnerable to cerebral I/R injury. Thus, intriguingly, the present study supports the possibility of utilizing an intranasal caspase-1 inhibitor as an effective treatment for post-cardiac arrest cerebral I/R injury.

We firstly characterized the cell type of expression of caspase-1 in the non-ischemic hippocampal CA1 region and its temporal pattern following the ischemic states. Our studies

Author Manuscript Author Manuscript Author Manuscript Author Manuscript

revealed that, under basal condition (sham-operated animals), caspase-1 is mainly expressed in CA1 pyramidal neurons, with less co-localization/expression observed in astroglial cells. In contrast, at 3 days and 14 days after ischemic reperfusion, the situation is reversed, with caspase-1 expression predominantly observed in reactive astrocytes. We also found that caspase-1 activity was significantly elevated 2 days following GCI reperfusion, and reached its peak level at 3 days after reperfusion. This differs from the previous report that neuronal caspase-1 is activated rapidly within 30 min following a mouse model of MCAO [51]. Research in the same model has also shown that a caspase-1 inhibitor is neuroprotective after MCAO in rats when injected i.c.v. up to 3 hour following reperfusion [22]. However, due to the significant differences between the MCAO and GCI models, a separate time course was required for this study in order to determine the appropriate timing of drug administration and the measurement of caspase-1 activity in the setting of GCI. In this study, intranasally administered Boc-D-CMK inhibited both caspase-1 activity and overexpression in the hippocampual CA1 region. As previous studies have demonstrated, caspase-1 is directly involved in non-infectious cell death processes, such as those induced by hypoxia and ischemia [22,16]. Our current study, in the GCI model, extended previous reports regarding the role of caspase-1 in cerebral ischemia.

The precise molecular mechanisms underlying brain I/R injury remain unclear. However, as the current study suggests, neuro-inflammation and disruption of mitochondrial function appear to be the primary culprits of I/R injury after GCI. First, neuro-inflammation is triggered by I/R, leading to disruption of the BBB and delayed neuronal death in areas particularly vulnerable to ischemia, such as the hippocampal CA1 region. Neuroinflammation is heralded by the release of cytotoxic agents, including ROS, cytokines, nitric oxide, and matrix metalloproteinases [52]. Subsequently, cells affected by these insults release more toxic mediators, thereby activating more immune cells, which release more toxic, inflammatory substances. This vicious neuroinflammatory cascade results in prolonged inflammation that exacerbates the original injury induced by I/R after GCI [53]. Mitochondrial dysfunction is also triggered following I/R. Mitochondria typically consume 85% of the cell’s oxygen during its generation of ATP, producing 90% of the cell’s energy via oxidative phosphorylation. Arrest of the blood supply prevents delivery of oxygen and glucose to the highly metabolic brain and disrupts the mitochondria’s ATP production and oxidative phosphorylation. The subsequent reduction in cellular ATP limits the pumping ability of ion channels in the neuronal membrane, which ultimately induces mitochondrial damage. In brief, the mitochondria regulate membrane potential, ATP levels, calcium load, and apoptotic pathways, all of which play a central role in the development of I/R injury. Furthermore, PARP1, a genomic stability enzyme, responds to ischemia-induced DNA damage, leading to detrimental cytosolic NAD+ consumption, glycolytic inhibition, ATP depletion, mitochondrial permeability, and cell death [54,55]. The opening of the membrane permeability transition pore ultimately leads to mitochondrial dysfunction, oxidative stress, and caspase 3 dependent apoptotic cell death [56,57].

Considering that the caspase-1 inhibitor Boc-D-CMK has no direct inhibitory effect on caspase-3 *in vitro* [58], we aimed to determine whether and how the caspase-1 inhibitor might inhibit caspase-9 and caspase-3 apoptotic pathway *in vivo*. We found that Boc-D-CMK preserved the mitochondrial membrane potential following GCI, as examined by the

Author Manuscript Author Manuscript Author Manuscript Author Manuscript

MitoTracker Red staining. Boc-D-CMK treatment also significantly rescued I/R-induced decrease of cytochrome c oxidase activity in the hippocampal CA1 region. Importantly, inhibition of caspase-1 was able to effectively reduce the release of cytochrome c from mitochondria to the cytosol. All these observations support the ability of caspase-1 inhibition in attenuating mitochondrial dysfunction and maintaining healthy mitochondrial function in hippocampal CA1 neurons. In addition, Boc-D-CMK markedly prevented the neuronal activation of caspase-9 and caspase-3 proteases induced by GCI reperfusion, downstream of cytochrome c release. Consistent with the inhibitory effects on caspase activation, there was a gross reduction in the number of apoptotic cells and PARP1-positive cells, as shown by TUNEL and PARP1 staining, respectively, in CA1 region following GCI. Reactive gliosis induced by ischemia insult could lead to oxidative stress and neuroinflammation and result in local microenvironment changes, to feedback stimulate neuronal damage. It is well recognized that oxidative stress and inflammation are closely linked to mitochondrial dysfunction in neuronal degenerative condition [59–61]. Concomitantly, Boc-D-CMK treated animals show reduced reactive gliosis and the pro-inflammatory cytokines production, such as IL-1β , IL-18, IL-6 and TNF-α 3 days after GCI. Intriguingly, these cytokines are the downstream inflammatory cytokines of caspase-1 in rats subjected to GCI, and are known to be contributing factors of autophagic death [62–64]. Taken together, intranasal Boc-D-CMK administration has the ability to attenuate neuronal apoptosis following GCI by preserving MMP, rescuing GCI-induced decreases of cytochrome c oxidase activity, and then inhibiting the caspase 3 dependent intrinsic apoptotic pathways. Importantly, caspase-1 is not only implied as a key mediator of inflammatory processes but also as a key executioner of apoptosis.

Delayed cell loss of CA1 hippocampal neurons is known to occur after transient GCI [65,66]. In the present study, a 4-vessel occlusion rat model of GCI was adopted, wherein the delayed neuronal death is severe in the CA1 subfield, and the CA3/DG cell layers are relatively resistant to GCI. This well characterized GCI model mimics the brain damage patterns observed in patients who experience cardiac arrest. We demonstrated that intranasal post-treatment with the caspase-1 inhibitor Boc-D-CMK protected vulnerable CA1 neurons in GCI, as confirmed by both Cresyl Violet staining and NeuN staining. Furthermore, using the Barnes maze test, our studies revealed that intranasal Boc-D-CMK post-treatment significantly attenuated functional impairments in spatial learning and memory following GCI. Deficits in cognitive functioning are a well-known comorbidity in those who survive cardiac arrest, whose episodic long-term memory appears to be particularly impaired [67]. In contrast, however, research concerning recognition memory impairment induced by transient GCI is scarce. Therefore, we also evaluated non-spatial recognition memory through the NOR task, which showed that intranasal Boc-D-CMK post-treatment significantly ameliorated the recognition memory loss observed after GCI. Thus, our data suggest that hippocampal integrity is necessary for recognition memory, as previously reported [47]. Altogether, these research findings clearly support that Boc-D-CMK induces neuroprotection and prevents neurocognitive impairment in the setting of transient GCI.

In conclusion, the results of the current study demonstrate that intranasal post-treatment with the caspase-1 inhibitor Boc-D-CMK attenuates hippocampal neuronal loss and improves neurocognitive outcomes, with respect to both spatial and non-spatial learning/memory, after

Author Manuscript Author Manuscript Author Manuscript Author Manuscript

GCI in rats. These are associated with preservation of mitochondrial function, prevention of the harmful neuroinflammation, and prevention of the activation of the final apoptotic executioner, caspase-3. Therefore, the protective effects may potentially occur through dual inhibition of both caspase-dependent apoptosis and pro-inflammatory cytokines triggered neuronal apoptosis following GCI. Altogether, our findings indicate that intranasal Boc-D-CMK post-treatment could serve as a promising clinical therapeutic strategy to address neurological insults incurred as a result of cardiac arrest and resuscitation. However, since the precise mechanism underlying the functional role of caspase-1 inhibitors in cerebral ischemia remains unclear, further study is warranted prior to progressing to the clinical arena.

Acknowledgments

This study was supported by Research Grant NS086929 from the National Institute of Neurological Disorders and Stroke, National Institutes of Health, USA; an American Heart Association Grant-in-Aid 15GRNT25240004; and by the Priority Academic Program Development of Jiangsu Higher Education Institutions & Open project of Key Laboratory of Brain Diseases Bioimformation (Xuzhou Medical University, JSBL1406), and the Jiangsu Government Scholarship Fund (JS2013245).

References

1. Mozaffarian D, Benjamin EJ, Go AS, Arnett DK, Blaha MJ, Cushman M, de Ferranti S, Despres JP, Fullerton HJ, Howard VJ, Huffman MD, Judd SE, Kissela BM, Lackland DT, Lichtman JH, Lisabeth LD, Liu S, Mackey RH, Matchar DB, McGuire DK, Mohler ER 3rd, Moy CS, Muntner P, Mussolino ME, Nasir K, Neumar RW, Nichol G, Palaniappan L, Pandey DK, Reeves MJ, Rodriguez CJ, Sorlie PD, Stein J, Towfighi A, Turan TN, Virani SS, Willey JZ, Woo D, Yeh RW, Turner MB. Heart disease and stroke statistics--2015 update: a report from the American Heart Association. Circulation. 2015; 131(4):e29–e322. [PubMed: 25520374]
2. Vereczki V, Martin E, Rosenthal RE, Hof PR, Hoffman GE, Fiskum G. Normoxic resuscitation after cardiac arrest protects against hippocampal oxidative stress, metabolic dysfunction, and neuronal death. Journal of cerebral blood flow and metabolism : official journal of the International Society of Cerebral Blood Flow and Metabolism. 2006; 26(6):821–835.
3. Safar P. Cerebral resuscitation after cardiac arrest: research initiatives and future directions. Annals of emergency medicine. 1993; 22(2 Pt 2):324–349. [PubMed: 8434832]
4. Zhang QG, Han D, Wang RM, Dong Y, Yang F, Vadlamudi RK, Brann DW. C terminus of Hsc70-interacting protein (CHIP)-mediated degradation of hippocampal estrogen receptor-alpha and the critical period hypothesis of estrogen neuroprotection. Proceedings of the National Academy of Sciences of the United States of America. 2011; 108(35):E617–E624. [PubMed: 21808025]
5. Safar P. Cerebral resuscitation after cardiac arrest: a review. Circulation. 1986; 74(6 Pt 2):IV138–IV153. [PubMed: 3536160]
6. Harukuni I, Bhardwaj A. Mechanisms of brain injury after global cerebral ischemia. Neurologic clinics. 2006; 24(1):1–21. [PubMed: 16443127]
7. Lipton P. Ischemic cell death in brain neurons. Physiological reviews. 1999; 79(4):1431–1568. [PubMed: 10508238]
8. Abe K, Aoki M, Kawagoe J, Yoshida T, Hattori A, Kogure K, Itoyama Y. Ischemic delayed neuronal death. A mitochondrial hypothesis. Stroke; a journal of cerebral circulation. 1995; 26(8):1478–1489.
9. Burke DT, Shah MK, Dorvlo AS, Al-Adawi S. Rehabilitation outcomes of cardiac and non-cardiac anoxic brain injury: a single institution experience. Brain injury. 2005; 19(9):675–680. [PubMed: 16195180]
10. Silva BC, de Miranda AS, Rodrigues FG, Silveira AL, Resende GH, Moraes MF, de Oliveira AC, Parreiras PM, Barcelos Lda S, Teixeira MM, Machado FS, Teixeira AL, Rachid MA. The 5-lipoxygenase (5-LOX) Inhibitor Zileuton Reduces Inflammation and Infarct Size with

Author Manuscript Author Manuscript Author Manuscript Author Manuscript

Improvement in Neurological Outcome Following Cerebral Ischemia. Current neurovascular research. 2015; 12(4):398–403. [PubMed: 26265153]

11. Onetti Y, Dantas AP, Perez B, Cugota R, Chamorro A, Planas AM, Vila E, Jimenez-Altayo F. Middle cerebral artery remodeling following transient brain ischemia is linked to early postischemic hyperemia: a target of uric acid treatment. American journal of physiology Heart and circulatory physiology. 2015; 308(8):H862–H874. [PubMed: 25637543]
12. Shao ZQ, Liu ZJ. Neuroinflammation and neuronal autophagic death were suppressed via Rosiglitazone treatment: New evidence on neuroprotection in a rat model of global cerebral ischemia. Journal of the neurological sciences. 2015; 349(1–2):65–71. [PubMed: 25623802]
13. Alnemri ES, Livingston DJ, Nicholson DW, Salvesen G, Thornberry NA, Wong WW, Yuan J. Human ICE/CED-3 protease nomenclature. Cell. 1996; 87(2):171. [PubMed: 8861900]
14. Thornberry NA, Bull HG, Calaycay JR, Chapman KT, Howard AD, Kostura MJ, Miller DK, Molineaux SM, Weidner JR, Aunins J, et al. A novel heterodimeric cysteine protease is required for interleukin-1 beta processing in monocytes. Nature. 1992; 356(6372):768–774. [PubMed: 1574116]
15. Howard AD, Kostura MJ, Thornberry N, Ding GJ, Limjuco G, Weidner J, Salley JP, Hogquist KA, Chaplin DD, Mumford RA, et al. IL-1-converting enzyme requires aspartic acid residues for processing of the IL-1 beta precursor at two distinct sites and does not cleave 31-kDa IL-1 alpha. J Immunol. 1991; 147(9):2964–2969. [PubMed: 1919001]
16. Zhang WH, Wang X, Narayanan M, Zhang Y, Huo C, Reed JC, Friedlander RM. Fundamental role of the Rip2/caspase-1 pathway in hypoxia and ischemia-induced neuronal cell death. Proceedings of the National Academy of Sciences of the United States of America. 2003; 100(26):16012–16017. [PubMed: 14663141]
17. Guegan C, Vila M, Teismann P, Chen C, Onteniente B, Li M, Friedlander RM, Przedborski S. Instrumental activation of bid by caspase-1 in a transgenic mouse model of ALS. Molecular and cellular neurosciences. 2002; 20(4):553–562. [PubMed: 12213439]
18. Li M, Ona VO, Guegan C, Chen M, Jackson-Lewis V, Andrews LJ, Olszewski AJ, Stieg PE, Lee JP, Przedborski S, Friedlander RM. Functional role of caspase-1 and caspase-3 in an ALS transgenic mouse model. Science. 2000; 288(5464):335–339. [PubMed: 10764647]
19. Willingham SB, Bergstralh DT, O'Connor W, Morrison AC, Taxman DJ, Duncan JA, Barnoy S, Venkatesan MM, Flavell RA, Deshmukh M, Hoffman HM, Ting JP. Microbial pathogen-induced necrotic cell death mediated by the inflammasome components CIAS1/cryopyrin/NLRP3 and ASC. Cell host & microbe. 2007; 2(3):147–159. [PubMed: 18005730]
20. Pasinelli P, Borchelt DR, Houseweart MK, Cleveland DW, Brown RH Jr. Caspase-1 is activated in neural cells and tissue with amyotrophic lateral sclerosis-associated mutations in copper-zinc superoxide dismutase. Proceedings of the National Academy of Sciences of the United States of America. 1998; 95(26):15763–15768. [PubMed: 9861044]
21. Kozai TD, Li X, Bodily LM, Caparosa EM, Zenonos GA, Carlisle DL, Friedlander RM, Cui XT. Effects of caspase-1 knockout on chronic neural recording quality and longevity: insight into cellular and molecular mechanisms of the reactive tissue response. Biomaterials. 2014; 35(36):9620–9634. [PubMed: 25176060]
22. Ross J, Brough D, Gibson RM, Loddick SA, Rothwell NJ. A selective, non-peptide caspase-1 inhibitor, VRT-018858, markedly reduces brain damage induced by transient ischemia in the rat. Neuropharmacology. 2007; 53(5):638–642. [PubMed: 17845807]
23. Rabuffetti M, Sciorati C, Tarozzo G, Clementi E, Manfredi AA, Beltramo M. Inhibition of caspase-1-like activity by Ac-Tyr-Val-Ala-Asp-chloromethyl ketone induces long-lasting neuroprotection in cerebral ischemia through apoptosis reduction and decrease of proinflammatory cytokines. The Journal of neuroscience : the official journal of the Society for Neuroscience. 2000; 20(12):4398–4404. [PubMed: 10844008]
24. Ray AM, Owen DE, Evans ML, Davis JB, Benham CD. Caspase inhibitors are functionally neuroprotective against oxygen glucose deprivation induced CA1 death in rat organotypic hippocampal slices. Brain research. 2000; 867(1–2):62–69. [PubMed: 10837798]
25. Zhang QG, Wang RM, Scott E, Han D, Dong Y, Tu JY, Yang F, Reddy Sareddy G, Vadlamudi RK, Brann DW. Hypersensitivity of the hippocampal CA3 region to stress-induced neurodegeneration

Author Manuscript Author Manuscript Author Manuscript Author Manuscript

and amyloidogenesis in a rat model of surgical menopause. Brain : a journal of neurology. 2013; 136(Pt 5):1432–1445.

26. Migliore MM, Vyas TK, Campbell RB, Amiji MM, Waszczak BL. Brain delivery of proteins by the intranasal route of administration: a comparison of cationic liposomes versus aqueous solution formulations. Journal of pharmaceutical sciences. 2010; 99(4):1745–1761. [PubMed: 19774660]
27. Thorne RG, Pronk GJ, Padmanabhan V, Frey WH 2nd. Delivery of insulin-like growth factor-I to the rat brain and spinal cord along olfactory and trigeminal pathways following intranasal administration. Neuroscience. 2004; 127(2):481–496. [PubMed: 15262337]
28. Zhang QG, Raz L, Wang R, Han D, De Sevilla L, Yang F, Vadlamudi RK, Brann DW. Estrogen attenuates ischemic oxidative damage via an estrogen receptor alpha-mediated inhibition of NADPH oxidase activation. The Journal of neuroscience : the official journal of the Society for Neuroscience. 2009; 29(44):13823–13836. [PubMed: 19889994]
29. Han D, Scott EL, Dong Y, Raz L, Wang R, Zhang Q. Attenuation of mitochondrial and nuclear p38alpha signaling: a novel mechanism of estrogen neuroprotection in cerebral ischemia. Molecular and cellular endocrinology. 2015; 400:21–31. [PubMed: 25462588]
30. Lu Q, Tucker D, Dong Y, Zhao N, Zhang Q. Neuroprotective and Functional Improvement Effects of Methylene Blue in Global Cerebral Ischemia. Molecular neurobiology. 2015
31. Gan SD, Patel KR. Enzyme immunoassay and enzyme-linked immunosorbent assay. The Journal of investigative dermatology. 2013; 133(9):e12. [PubMed: 23949770]
32. Ferguson SA, Law CD, Abshire JS. Developmental treatment with bisphenol A causes few alterations on measures of postweaning activity and learning. Neurotoxicology and teratology. 2012; 34(6):598–606. [PubMed: 23041373]
33. Barnes CA. Memory deficits associated with senescence: a neurophysiological and behavioral study in the rat. Journal of comparative and physiological psychology. 1979; 93(1):74–104. [PubMed: 221551]
34. Ennaceur A, Delacour J. A new one-trial test for neurobiological studies of memory in rats. 1: Behavioral data. Behavioural brain research. 1988; 31(1):47–59. [PubMed: 3228475]
35. Steckler T, Drinkenburg WH, Sahgal A, Aggleton JP. Recognition memory in rats--I. Concepts and classification. Progress in neurobiology. 1998; 54(3):289–311. [PubMed: 9481800]
36. Ennaceur A, Aggleton JP. Spontaneous recognition of object configurations in rats: effects of fornix lesions. Experimental brain research. 1994; 100(1):85–92. [PubMed: 7813656]
37. de Lima MN, Laranja DC, Bromberg E, Roesler R, Schroder N. Pre- or post-training administration of the NMDA receptor blocker MK-801 impairs object recognition memory in rats. Behavioural brain research. 2005; 156(1):139–143. [PubMed: 15474658]
38. Botton PH, Costa MS, Ardais AP, Mioranzza S, Souza DO, da Rocha JB, Porciuncula LO. Caffeine prevents disruption of memory consolidation in the inhibitory avoidance and novel object recognition tasks by scopolamine in adult mice. Behavioural brain research. 2010; 214(2):254–259. [PubMed: 20553765]
39. Gaskin S, Tardif M, Cole E, Piterkin P, Kayello L, Mumby DG. Object familiarization and novel-object preference in rats. Behavioural processes. 2010; 83(1):61–71. [PubMed: 19874876]
40. Kalogeris T, Bao Y, Korthuis RJ. Mitochondrial reactive oxygen species: a double edged sword in ischemia/reperfusion vs preconditioning. Redox biology. 2014; 2:702–714. [PubMed: 24944913]
41. Sanderson TH, Reynolds CA, Kumar R, Przyklenk K, Huttemann M. Molecular mechanisms of ischemia-reperfusion injury in brain: pivotal role of the mitochondrial membrane potential in reactive oxygen species generation. Molecular neurobiology. 2013; 47(1):9–23. [PubMed: 23011809]
42. Schroder K, Tschopp J. The inflammasomes. Cell. 2010; 140(6):821–832. [PubMed: 20303873]
43. Hentze H, Lin XY, Choi MS, Porter AG. Critical role for cathepsin B in mediating caspase-1-dependent interleukin-18 maturation and caspase-1-independent necrosis triggered by the microbial toxin nigericin. Cell death and differentiation. 2003; 10(9):956–968. [PubMed: 12934070]
44. Cohen RM, Rezai-Zadeh K, Weitz TM, Rentsendorj A, Gate D, Spivak I, Bholat Y, Vasilevko V, Glabe CG, Breunig JJ, Rakic P, Davtyan H, Agadjanyan MG, Kepe V, Barrio JR, Bannykh S, Szekely CA, Pechnick RN, Town T. A transgenic Alzheimer rat with plaques, tau pathology,

Author Manuscript Author Manuscript Author Manuscript Author Manuscript

behavioral impairment, oligomeric abeta, and frank neuronal loss. The Journal of neuroscience : the official journal of the Society for Neuroscience. 2013; 33(15):6245–6256. [PubMed: 23575824]

45. Barnes CA, Jung MW, McNaughton BL, Korol DL, Andreasson K, Worley PF. LTP saturation and spatial learning disruption: effects of task variables and saturation levels. The Journal of neuroscience : the official journal of the Society for Neuroscience. 1994; 14(10):5793–5806. [PubMed: 7931545]
46. Goodrich-Hunsaker NJ, Hunsaker MR, Kesner RP. The interactions and dissociations of the dorsal hippocampus subregions: how the dentate gyrus, CA3, and CA1 process spatial information. Behavioral neuroscience. 2008; 122(1):16–26. [PubMed: 18298245]
47. Broadbent NJ, Squire LR, Clark RE. Spatial memory, recognition memory, and the hippocampus. Proceedings of the National Academy of Sciences of the United States of America. 2004; 101(40): 14515–14520. [PubMed: 15452348]
48. Liu XF, Fawcett JR, Hanson LR, Frey WH 2nd. The window of opportunity for treatment of focal cerebral ischemic damage with noninvasive intranasal insulin-like growth factor-I in rats. Journal of stroke and cerebrovascular diseases : the official journal of National Stroke Association. 2004; 13(1):16–23. [PubMed: 17903945]
49. De Rosa R, Garcia AA, Braschi C, Capsoni S, Maffei L, Berardi N, Cattaneo A. Intranasal administration of nerve growth factor (NGF) rescues recognition memory deficits in AD11 anti-NGF transgenic mice. Proceedings of the National Academy of Sciences of the United States of America. 2005; 102(10):3811–3816. [PubMed: 15728733]
50. Capsoni S, Giannotta S, Cattaneo A. Nerve growth factor and galantamine ameliorate early signs of neurodegeneration in anti-nerve growth factor mice. Proceedings of the National Academy of Sciences of the United States of America. 2002; 99(19):12432–12437. [PubMed: 12205295]
51. Benchoua A, Guegan C, Couriaud C, Hosseini H, Sampaio N, Morin D, Onteniente B. Specific caspase pathways are activated in the two stages of cerebral infarction. The Journal of neuroscience : the official journal of the Society for Neuroscience. 2001; 21(18):7127–7134. [PubMed: 11549723]
52. Stoll G, Kleinschnitz C, Nieswandt B. Combating innate inflammation: a new paradigm for acute treatment of stroke? Annals of the New York Academy of Sciences. 2010; 1207:149–154. [PubMed: 20955438]
53. Danton GH, Dietrich WD. Inflammatory mechanisms after ischemia and stroke. Journal of neuropathology and experimental neurology. 2003; 62(2):127–136. [PubMed: 12578222]
54. Lu P, Kamboj A, Gibson SB, Anderson CM. Poly(ADP-ribose) polymerase-1 causes mitochondrial damage and neuron death mediated by Bnip3. The Journal of neuroscience : the official journal of the Society for Neuroscience. 2014; 34(48):15975–15987. [PubMed: 25429139]
55. Cohen A, Barankiewicz J. Metabolic consequences of DNA damage: alteration in purine metabolism following poly(ADP ribosyl)ation in human T-lymphoblasts. Archives of biochemistry and biophysics. 1987; 258(2):498–503. [PubMed: 2960266]
56. Andrabi SA, Kim NS, Yu SW, Wang H, Koh DW, Sasaki M, Klaus JA, Otsuka T, Zhang Z, Koehler RC, Hurn PD, Poirier GG, Dawson VL, Dawson TM. Poly(ADP-ribose) (PAR) polymer is a death signal. Proceedings of the National Academy of Sciences of the United States of America. 2006; 103(48):18308–18313. [PubMed: 17116882]
57. Yu SW, Andrabi SA, Wang H, Kim NS, Poirier GG, Dawson TM, Dawson VL. Apoptosis-inducing factor mediates poly(ADP-ribose) (PAR) polymer-induced cell death. Proceedings of the National Academy of Sciences of the United States of America. 2006; 103(48):18314–18319. [PubMed: 17116881]
58. Garcia-Calvo M, Peterson EP, Leiting B, Ruel R, Nicholson DW, Thornberry NA. Inhibition of human caspases by peptide-based and macromolecular inhibitors. The Journal of biological chemistry. 1998; 273(49):32608–32613. [PubMed: 9829999]
59. Freund-Levi Y, Vedin I, Hjorth E, Basun H, Faxen Irving G, Schultzberg M, Eriksdotter M, Palmblad J, Vessby B, Wahlund LO, Cederholm T, Basu S. Effects of supplementation with omega-3 fatty acids on oxidative stress and inflammation in patients with Alzheimer's disease: the OmegAD study. Journal of Alzheimer's disease : JAD. 2014; 42(3):823–831. [PubMed: 24934544]

Author Manuscript Author Manuscript Author Manuscript Author Manuscript

60. Urrutia PJ, Mena NP, Nunez MT. The interplay between iron accumulation, mitochondrial dysfunction, and inflammation during the execution step of neurodegenerative disorders. Frontiers in pharmacology. 2014; 5:38. [PubMed: 24653700]

61. Witte ME, Geurts JJ, de Vries HE, van der Valk P, van Horssen J. Mitochondrial dysfunction: a potential link between neuroinflammation and neurodegeneration? Mitochondrion. 2010; 10(5): 411–418. [PubMed: 20573557]

62. Dutta RK, Kathania M, Raje M, Majumdar S. IL-6 inhibits IFN-gamma induced autophagy in Mycobacterium tuberculosis H37Rv infected macrophages. The international journal of biochemistry & cell biology. 2012; 44(6):942–954. [PubMed: 22426116]

63. Shi CS, Shenderov K, Huang NN, Kabat J, Abu-Asab M, Fitzgerald KA, Sher A, Kehrl JH. Activation of autophagy by inflammatory signals limits IL-1beta production by targeting ubiquitinated inflammasomes for destruction. Nature immunology. 2012; 13(3):255–263. [PubMed: 22286270]

64. Jia G, Cheng G, Gangahar DM, Agrawal DK. Insulin-like growth factor-1 and TNF-αlpha regulate autophagy through c-jun N-terminal kinase and Akt pathways in human atherosclerotic vascular smooth cells. Immunology and cell biology. 2006; 84(5):448–454. [PubMed: 16942488]

65. Kirino T. Delayed neuronal death in the gerbil hippocampus following ischemia. Brain research. 1982; 239(1):57–69. [PubMed: 7093691]

66. Pulsinelli WA, Brierley JB, Plum F. Temporal profile of neuronal damage in a model of transient forebrain ischemia. Annals of neurology. 1982; 11(5):491–498. [PubMed: 7103425]

67. Sulzgruber P, Kliegel A, Wandaller C, Uray T, Losert H, Laggner AN, Sterz F, Kliegel M. Survivors of cardiac arrest with good neurological outcome show considerable impairments of memory functioning. Resuscitation. 2015; 88:120–125. [PubMed: 25461492]

Author Manuscript Author Manuscript Author Manuscript Author Manuscript

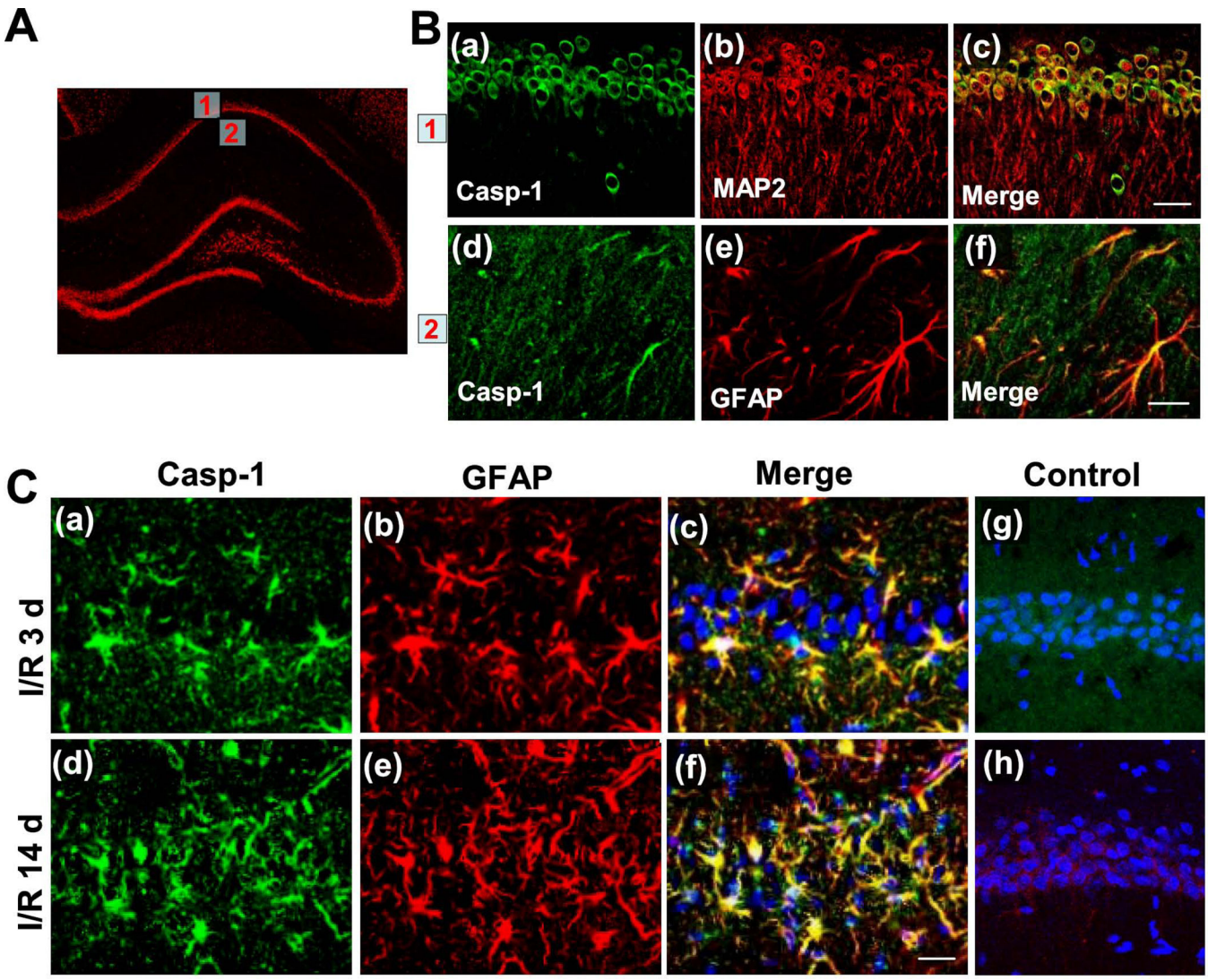

Fig. 1. Caspase-1 protein expression pattern in sham-operated rats and rats at 3 and 14 days after GCI in the hippocampal CA1 region

A, B Immunofluorescence staining for caspase-1, MAP2, GFAP and merged images of the hippocampal CA1 region in sham-operated rats. Boxed areas are pyramidal cell layer (1) and stratum radiatum (2) of medial CA1 region and shown in the right panel. **C** Confocal analysis for caspase-1, GFAP, DAPI and merged images of medial CA1 region 3 days (I/R 3d) and 14 days (I/R 14d) after GCI. Negative control staining for caspase-1 (Casp-1) and GFAP of the I/R 3 d CA1 region are shown in (g) and (h), respectively. Note that there was significant overexpression of caspase-1 protein in astrocytes both 3 days and 14 days following GCI. Representative confocal images are shown from 4–5 rats per group (magnification x40, scale bar 50 μm).

Author Manuscript Author Manuscript Author Manuscript Author Manuscript

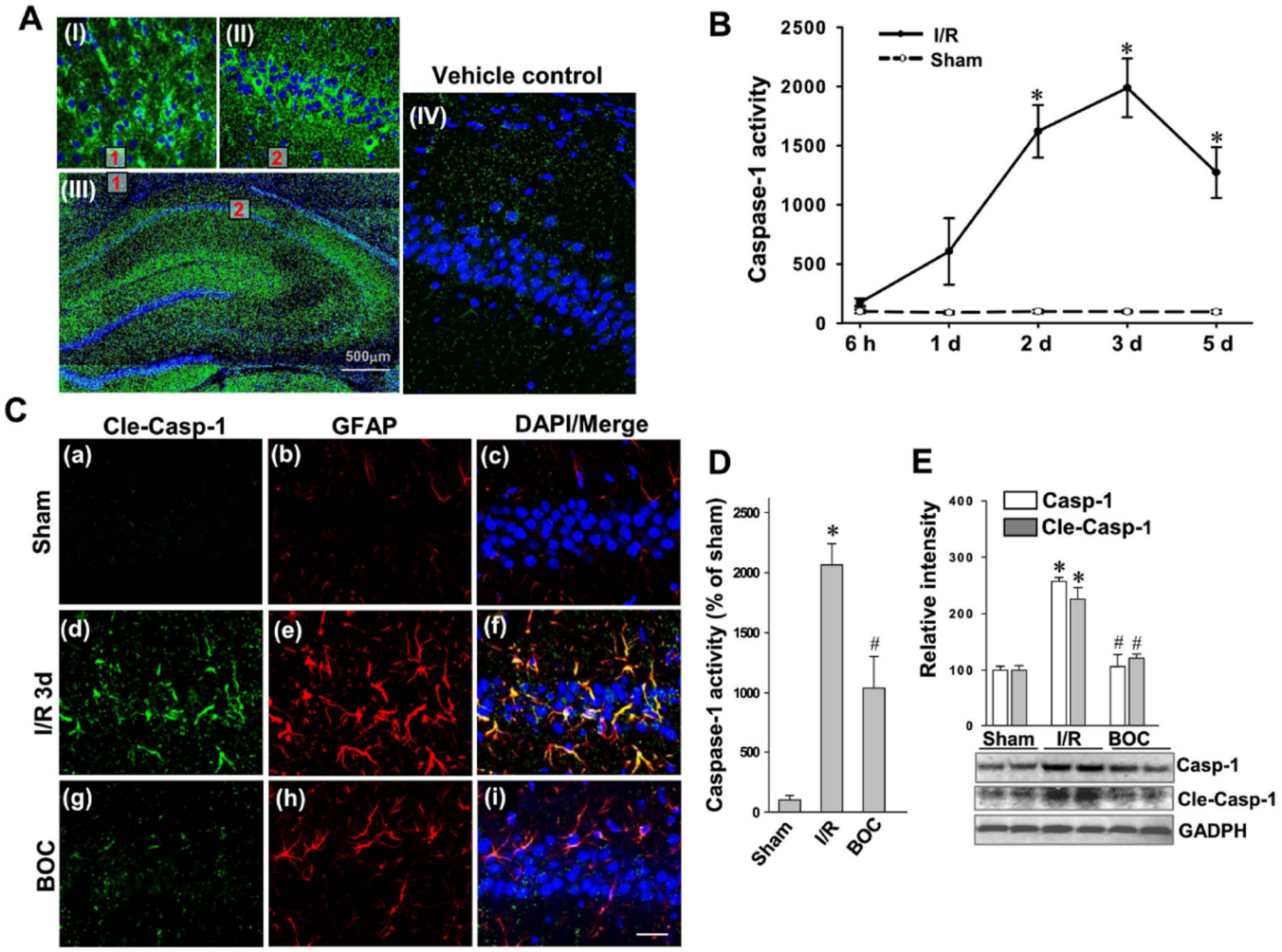

Fig. 2. Effect of Boc-D-CMK on caspase-1 activity, cleavage, and overexpression 3 days following GCI in the rat hippocampal CA1 region

A Representative confocal images showing neural distribution of biotin-labeled caspase-1 inhibitor 12 h after intranasal administration (Magnification x5, Scale bar 500 mm). Boxed areas in (III) are enlarged and shown in the up panel (I) and (II). Vehicle control received vehicle buffer is shown in (IV). **B** Caspase-1 activity from sham and I/R group at each time point was detected by a chromogenic substrate assay using hippocampal CA1 homogenates at the indicated time points post GCI. **C** Confocal microscopy of cleaved caspase-1 (Cle-Casp-1, green) and GFAP (red) staining taken from medial hippocampal CA1 region at day 3 after GCI. Representative images are shown from 4–5 rats per group (Magnification x40, Scale bar 50 μm). **D, E** Caspase-1 activity assay and Western blotting analyses of total caspase-1 and Cleaved caspase-1 expression 3 days after GCI in the hippocampal CA1 region. Data are presented as mean± SE, n= 5–6 per group. $^{*}P < 0.05$ vs. sham, $^{\#}P < 0.05$ vs. I/R group. BOC: Boc-D-CMK; I/R: ischemic reperfusion.

Author Manuscript
Author Manuscript
Author Manuscript
Author Manuscript

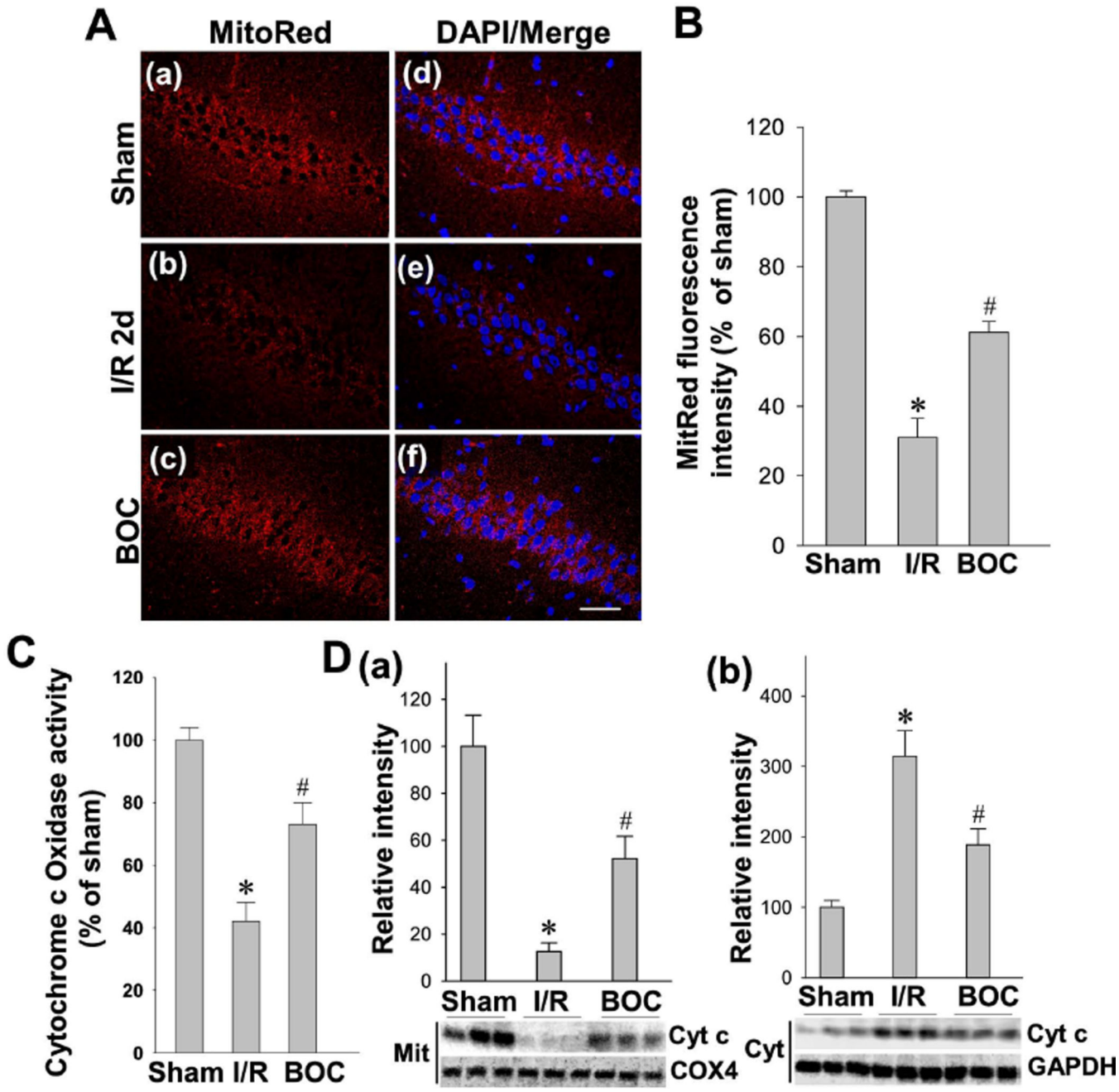

Fig. 3. Effect of Boc-D-CMK on depolarization of mitochondrial membrane potential (MMP), cytochrome c oxidase activity and cytochrome c release 2 days after GCI

A, B Representative confocal images and analysis for MitoTracker Red and DAPI in the hippocampal CA1 region 2 days after GCI (Magnification x40, Scale bar 50 μm). The fluorescence intensity of MitoTracker Red was measured and normalized as percentage changes versus sham group. MMP became hyperpolarized in I/R group at day 2, which was significantly recovered in the Boc-D-CMK-treated group. **C** Mitochaondrial cytochrome c oxidase activity was assessed on day 2 after GCI. **D** Western blotting and data analyses of cytochrome c levels using mitochondrial (Mit) and cytosolic (Cyt) protein samples. COX4 or

GADPH was used as loading controls. Data are expressed as mean ± SE, n= 4–5 per group. $^{*}P < 0.05$ vs. sham, $^{\#}P < 0.05$ vs. I/*R* group.

Author Manuscript Author Manuscript Author Manuscript Author Manuscript

Author Manuscript Author Manuscript Author Manuscript Author Manuscript

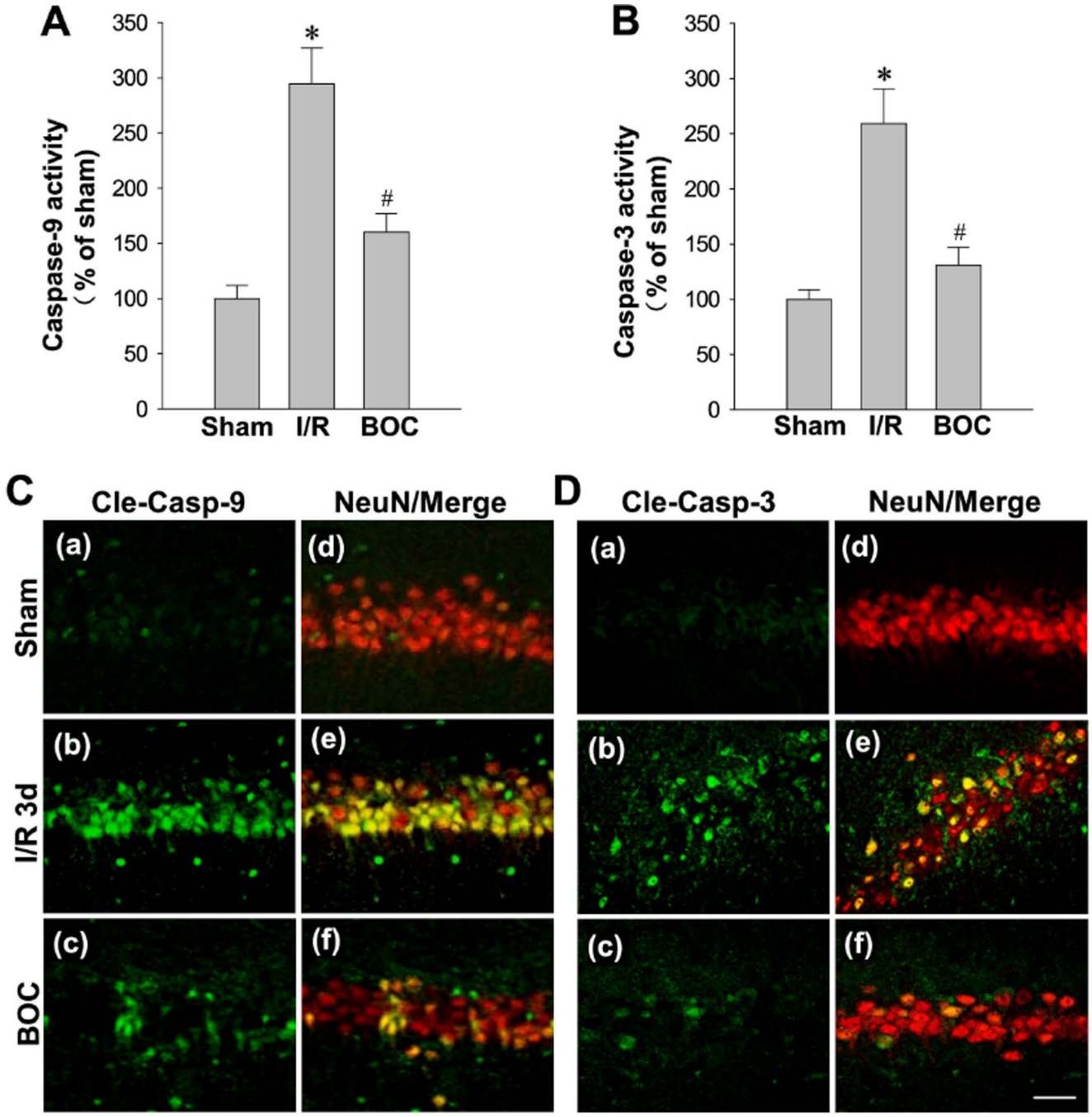

Fig. 4. Effect of Boc-D-CMK on the activation of caspase-9 and caspase-3 induced by I/R in hippocampal CA1 region

A, B The activities of caspase-9 and caspase-3 were measured by a fluorometric substrate assay using hippocampal CA1 homogenates 3 days after GCI. Data are presented as mean ±SE, n= 5–6 per group. $^{*}P < 0.05$ vs. sham, $^{\#}P < 0.05$ vs. I/R. **C, D** Representative confocal images showing the staining of cleaved caspase-9 and cleaved caspase-3 expression and their co-colocalizations with NeuN 3 days after I/R in medial CA1 region. Representative images represent 5–6 animals in each group. (Maginification x40, scale Bar 50 μm).

Author Manuscript Author Manuscript Author Manuscript Author Manuscript

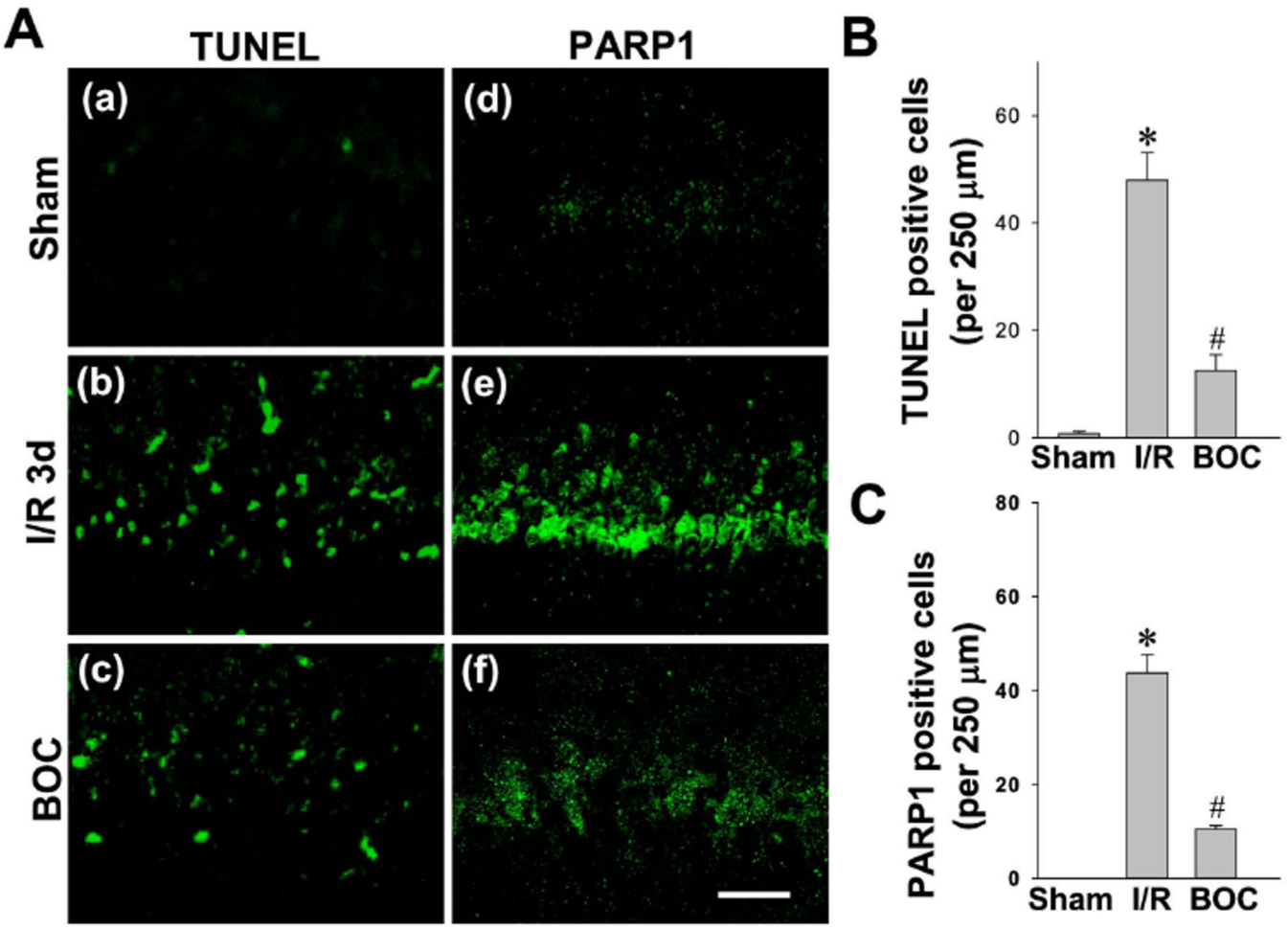

Fig. 5. Effect of Boc-D-CMK on neuronal apoptosis and PARP1 activation induced by I/R in hippocampal CA1 region

A Representative confocal microscopy images of TUNEL staining and PARP1 staining in the hippocampal CA1 region 3 days after GCI. **B, C** Cell-counting analyses of TUNEL-positive cells and PARP1-positive cells per 250 μm of medial CA1 region. Data are shown as mean±SE, n = 5–6 per group. $^{*}P < 0.05$ vs. sham, $^{\#}P < 0.05$ vs. I/*R*. (Magnification x40, scale Bar 50 μm).

Author Manuscript Author Manuscript Author Manuscript Author Manuscript

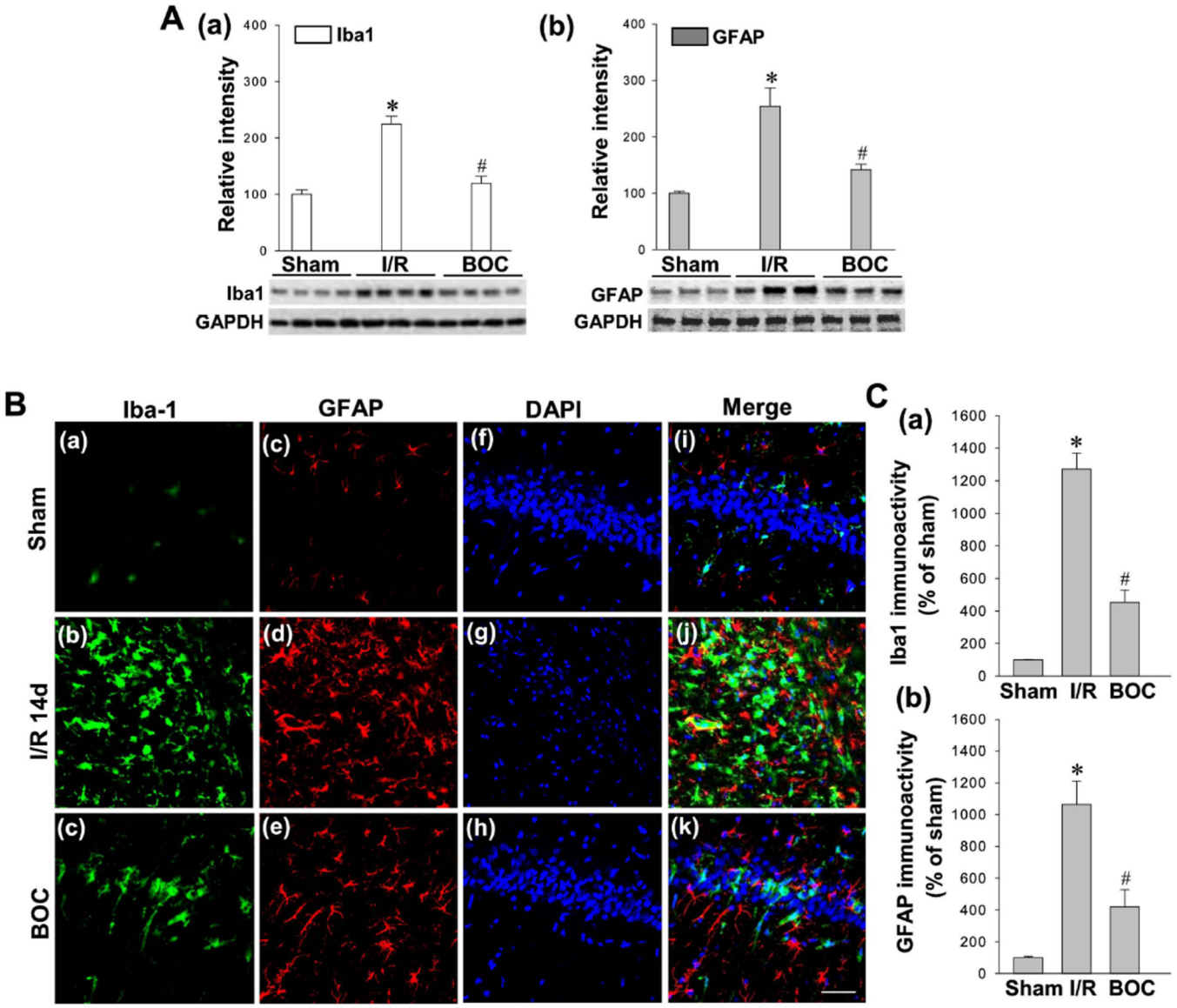

Fig. 6. Effect of Boc-D-CMK on GCI-induced reactive gliosis at the early and late stages after I/R

A Protein samples from hippocampal CA1 region 3 days post GCI were subjected to Western blotting analyses with antibodies specific for Iba1 and GFAP. Data are mean ± SE, n=4–5 per group. **B,C** Typical confocal microscopy images showing Iba-1 staining (Green), GFAP staining (Red) and DAPI staining (Blue) 14 days after I/R (Magnification x40, scale Bar 50 μm). The immunoactivity associated with Iba1 and GFAP were quantified and shown as percentage changes versus sham group. Data are presented as mean ± SE, n= 5–6 per group. $^{*}P<0.05$ vs. sham, $^{\#}P<0.05$ vs. I/R.

Author Manuscript Author Manuscript Author Manuscript Author Manuscript

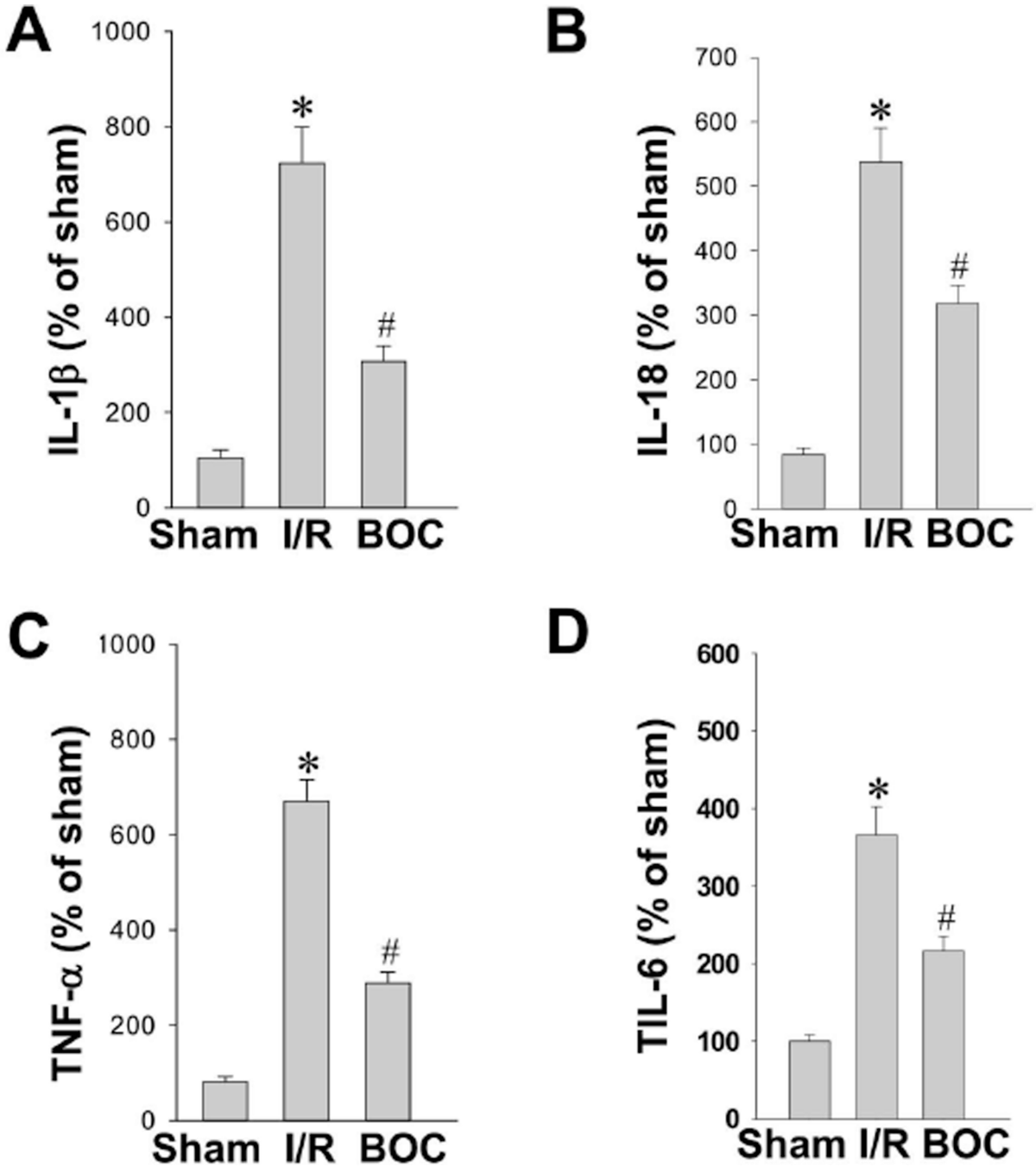

Fig. 7. Effect of Boc-D-CMK on pro-inflammatory cytokines production induced by I/R in hippocampal CA1 region

A–D ELISA assays of pro-inflammatory cytokines IL-1β, IL-18, TNF-α and IL-6 were performed using hippocampal CA1 homogenates 3 days after I/R. Data are expressed as means ± SE from 5–6 animals in each group and quantified as percentage changes versus sham controls. *P <0.05 vs. sham, $^{\#}$P <0.05 vs. I/R.

Author Manuscript Author Manuscript Author Manuscript Author Manuscript

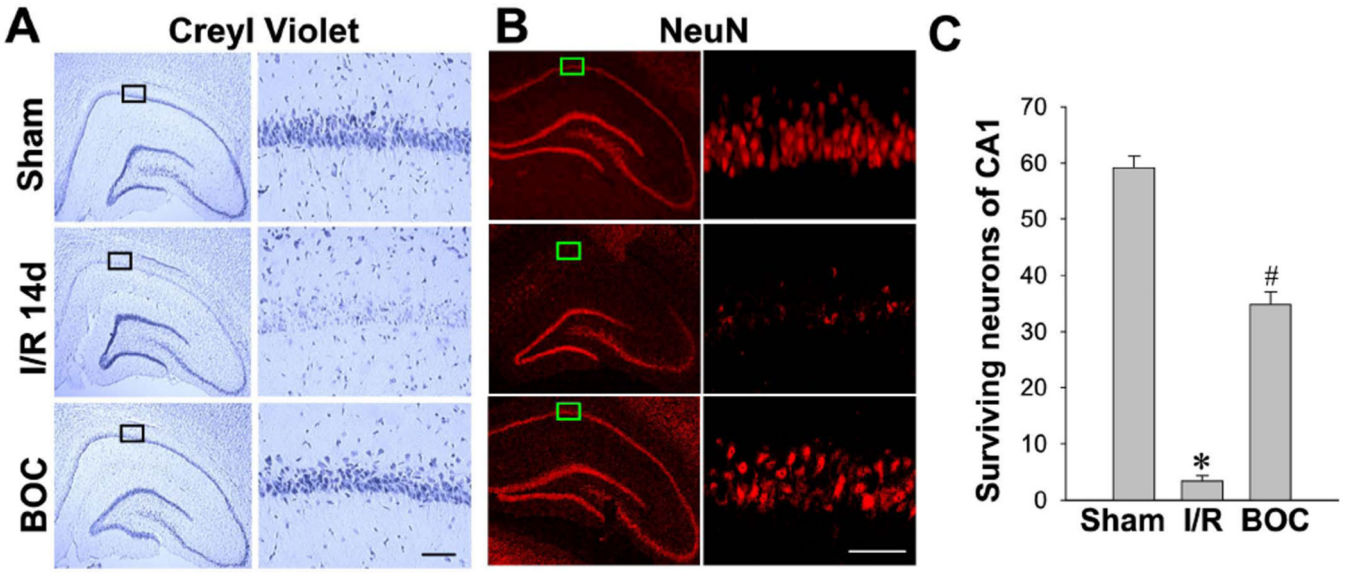

Fig. 8. Effect of Boc-D-CMK on delayed neuronal cell death induced by I/R in hippocampal CA1 region

A, B Representative images of Cresyl Violet staining and NeuN staining in the brain sections 14 days post I/R. NeuN-positive CA1 pyramidal cells showing intact and round nuclei as in sham animals were counted as surviving neurons. **C** Quantitative summary of data (mean±SE, n = 7–8 animals per group) showing the number of surviving neurons per 250 μm length of medial CA1 region. (Magnification: ×5 and *20 for Creyl violet, ×40 for NeuN, scale bar 50 μm.) $^{*}P<0.05$ vs. sham, $^{\#}P<0.05$ vs. I/R.

Author Manuscript Author Manuscript Author Manuscript Author Manuscript

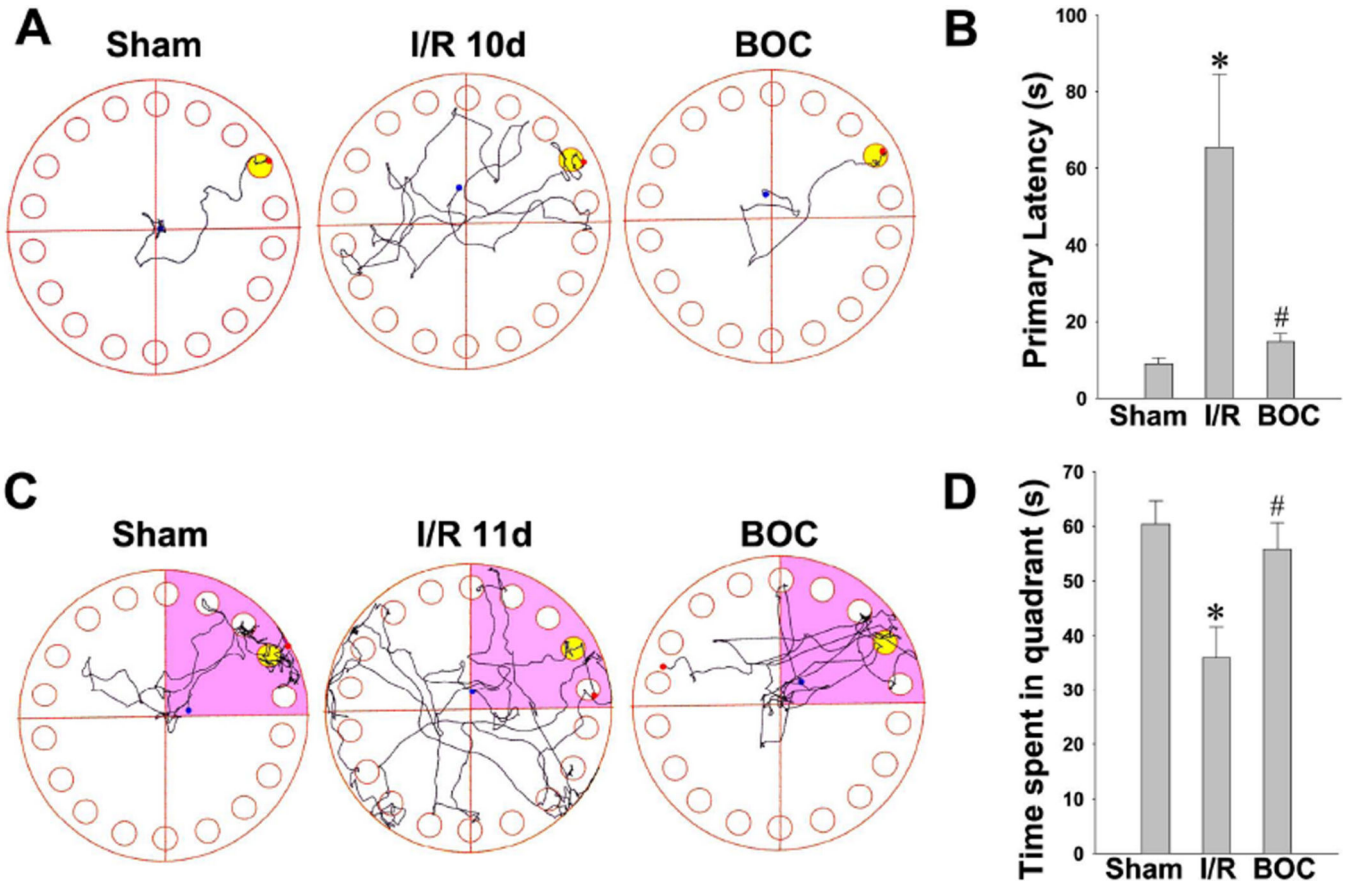

Fig. 9. Boc-D-CMK significantly attenuated learning and memory deficits induced by GCI

A, B The Barnes maze task was performed to test the spatial learning ability on day 8, 9 and 10 after I/R. Representative escaping traces of the indicated animals on day10 after GCI are shown in **A**. The escape latency to find the black hidden box was analyzed and shown in **B. C, D** Probe tests were performed on day 11 after GCI by removing the escape box and analyzing the total time spent exploring the target quadrant. The representative tracks in the quadrant zone are shown. Data are presented as mean±SE, n=7–8 per group. $^{*}P < 0.05$ vs. sham, $^{\#}P < 0.05$ vs. I/R.

Author Manuscript Author Manuscript Author Manuscript Author Manuscript

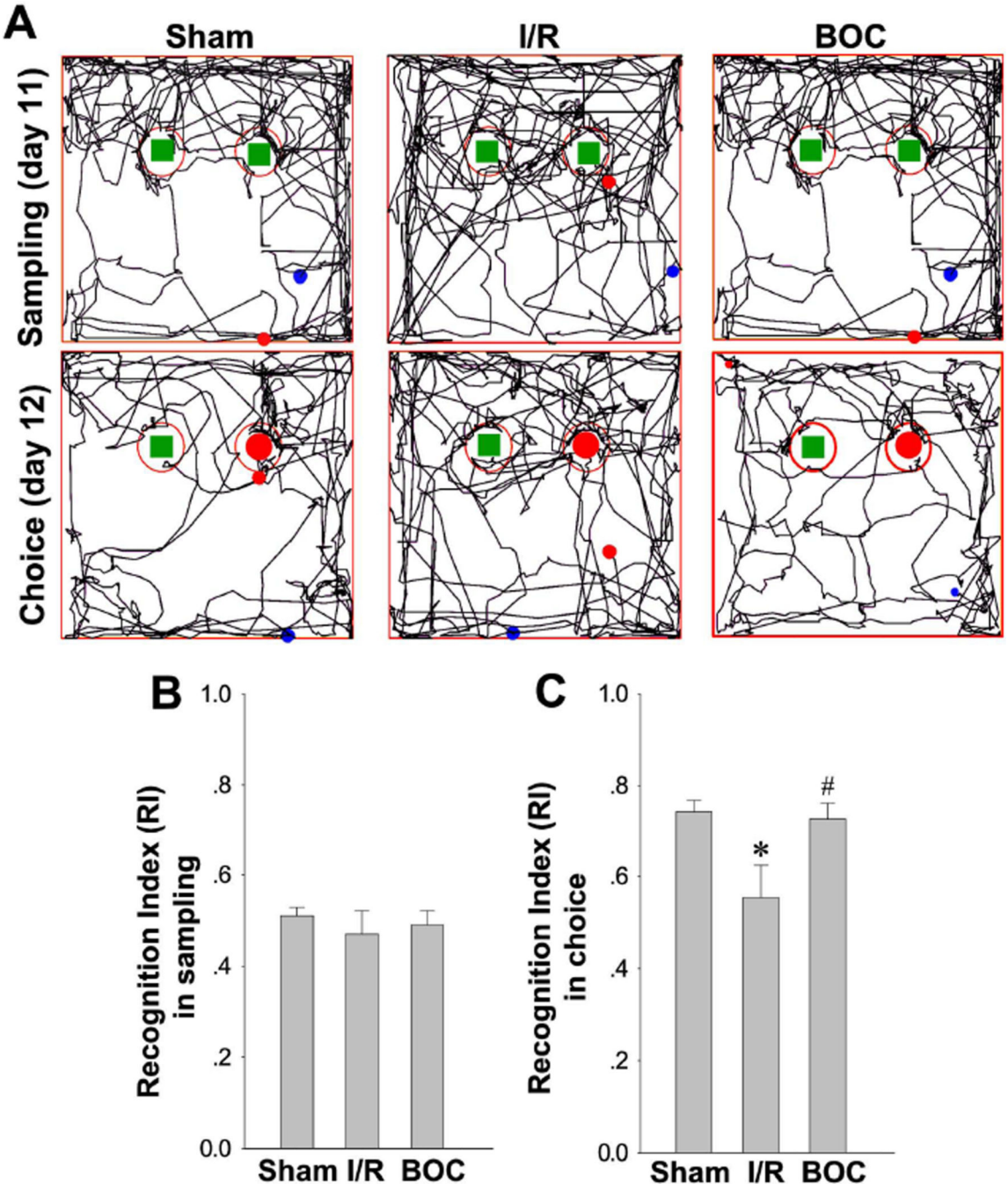

Fig. 10. Boc-D-CMK enhanced recognition memory in Novel Object Recognition test after GCI

A Novel Object Recognition tests after GCI were performed to monitor the long-term recognition memory. Representative traces in the sampling session to explore the familiar object on day 12 after GCI, and the choice session to explore the novel object on day 13 after GCI are shown. **B, C** Recognition index (RI) was calculated and statistically compared among all groups. Data are presented as mean±SE, n=7–8 per group. $^{*}P < 0.05$ vs. sham, $^{\#}P < 0.05$ vs. I/R.